2016

Surface Chemistry And Transport Properties Of II-VI Semiconductor Nanowires

Pravin Paudel
University of South Carolina

SURFACE CHEMISTRY AND TRANSPORT PROPERTIES OF II-VI SEMICONDUCTOR NANOWIRES

by

Pravin Paudel

Bachelor of Science
University of New Orleans, 2010

Submitted in Partial Fulfillment of the Requirements

For the Degree of Doctor of Philosophy in

Chemistry

College of Arts and Sciences

University of South Carolina

2016

Accepted by:

Andrew B Greytak, Major Professor

Thomas Vogt, Committee Member

Hui Wang, Committee Member

Krishna Mandal, Committee Member

Lacy Ford, Senior Vice Provost and Dean of Graduate Studies

DEDICATION

This thesis is dedicated to my parents Madhusudan Paudel and Yogamaya Paudel and my wife Neelam Maharjan.

ACKNOWLEDGEMENTS

Last five and half years are the most memorable time of my life. I met and worked with a lot of people, and learnt many things. This was the time I learnt about my life, more about chemistry and many non-chemistry related things. Coming to South Carolina without any background in electronics and semiconductors, I got to learn how they work. I cannot forget the first few years when I felt I was a plumber rather than a chemist because of various works related to tubing while setting up the lab. These moments were precious, and I need to acknowledge a lot of people who supported me through out these years.

First of all, I would like to thank my advisor Dr. Andrew B Greytak who supported me and helped me throughout this five and half years. He always provided constructive feedback, and motivated me. It is my great pleasure to have him as my advisor for my PhD research. I would also like to thank Dr. Thomas Vogt, Dr. Hui Wang, and Dr. Krishna Mandal for being my committee members and for providing helpful comments and encouragement. I also want to acknowledge the help from Dr. Linda Shimizu and Dr. MVS Chandrashekhar.

I want to thank my wonderful lab mates Bobby Barker, Preecha Kittikunnatham, Rui Tan, Yi Shen, Megan Gee, Adam Roberge, and Stephen Roberts. They are very amazing, and it is always a fun to work with them. I will also like to thank Christopher Pinion, Benjamin Gilbert and Aaron Cameron for their help.

I also want to thank my father and mother for their help, support, guidance and motivation throughout my life. I would not have been to this place without them. I also want to thank my wife, Neelam Maharjan for being with me. She left her job and career just to be with me. That means a lot to me. I am grateful for her dedications.

ABSTRACT

Semiconductor nanowires have been widely studied due to their unique properties such as width comparable to critical length-scales, high aspect ratio, and high carrier mobility. These unique properties make them a suitable candidate for various optical and electronic devices like photovoltaics, photodetectors, and field effect transistors. The nanowire surface plays an important role in the performance of these devices because of their high surface to volume ratio. The larger surface area of nanowires may provide better charge separation than planar heterostructures in photovoltaics by providing shorter distance to move for carrier before separation, however, presence of surface states may lead to the recombination of photo-generated carriers, limiting the amount of charge separation. In order to remove these surface states, ligands can be attached to the surface of nanowires.

In this work CdS and CdSe nanowires are grown through the high temperature Vapor-Liquid-Solid (VLS) process. VLS process yields single crystalline, low defect nanowires with controllable length and diameter. In order to show ligand binding on nanowire surface, CdS nanowires were treated with a dye-labeled polymer. Fluorescence microscopy and spectroscopy were used to confirm ligand binding. Fluorescence microscopy can also be used to show the kinetics of ligand binding on nanowire surfaces. In order to control the electronic properties of the nanowire surfaces, nanowires were treated with solution phase and vapor phase reagents.

Photoluminescence measurements and transport measurements were performed before and after the chemical treatment to see the consequences of ligand binding on the optical and electronic properties of nanowires.

TABLE OF CONTENTS

LIST OF FIGURES

LIST OF SYMBOLS

B	Available binding site on the nanowire surface.
BL	Occupied binding site on the nanowire surface.
$[BL]_e$	Concentration of ligand at equilibrium point when all the available sites are occupied.
$[BL]_t$	Concentration of bound ligand at particular time t.
K_a	Binding constant.
K_{off}	Desorption rate constant.
K_{on}	Adsorption rate constant.
K_{app}	Apparent rate constant.
L	Fluorescently labeled ligand.

List of Abbreviations

CdO ..... Cadmium oxide

CVD ..... Chemical Vapor Deposition

DMSO ..... Dimethyl Sulfoxide

FL ..... Fluorescence

HOMO ..... Highest Occupied Molecular Orbital

LUMO ..... Lowest Unoccupied Molecular Orbital

MBE ..... Molecular Beam Epitaxy

MW ..... Molecular Weight

PDA ..... Polydiacetylene

PDMS ..... Polydimethylsiloxane

PEG ..... Polyethylene Glycol

PL ..... Photoluminescence

QD ..... Quantum Dots

SEM ..... Scanning Electron Microscopy

SLS ..... Solution-Liquid-Solid

TEM ..... Transmission Electron Microscopy

TOPO ..... Trioctylphosphine Oxide

TOPS ..... Trioctylphosphine Sulfide

TOPSe ..... Trioctylphosphine Selenide

VLS ..... Vapor-Liquid-Solid

XPS .... X-ray Photoelectron Spectroscopy

CHAPTER 1

INTRODUCTION TO SEMICONDUCTOR NANOWIRES

1.1 NANOSCIENCE

Nanoscience is currently one of the most studied field of physics, chemistry, biology and engineering. It is a science that studies the structures and properties of materials at nanoscale size. It encompasses structures with critical dimensions of 1-1000 nm. Even though modern nanoscience is a half century old, nanostructures have always existed in mother nature. DNA, the building block of life, is around 2.5 nm in diameter. Similarly hemoglobin, a protein that transports oxygen, is around 5.5 nm. Across for hundreds of years, people have used different size of gold and silver nanoparticles to color the glass windows of medieval churches, even though they were unaware of nanoscience.

Modern nanoscience emerged after physicist Richard Feynman gave a talk at American physics society meeting on 1959.[1] His talk entitled "There's a Plenty of Room at the Bottom" was focused on the problem of manipulating and controlling things on a small scale. In his talk he said, "Why cannot we write the entire 24 volumes of the encyclopedia Britannica on the head of the pin?"[1] At present, because of his vision and motivation, his ideas are feasible. The discovery of electron microscopy in 1930s and scanning tunneling microscopy in 1980s provided an opportunity for scientists to study the morphology and growth of those nanostructures in more depth.

Reducing bulk materials to nanomaterials enhances various properties of materials such as higher strength, lighter weight, increased control of light spectrum, and greater chemical reactivity. This is because of two different reasons: size effect and quantum confinement effect.[2] Compared to the bulk, surface atoms of nanomaterials have lower co-ordination number and higher unsatisfied bond because of fewer neighboring atoms. The fraction of atoms at the surface and average binding energy per atom increases with the decrease in the size of nanoparticles. This brings different properties in nanomaterials compared to bulk. Similarly, in the bulk, electronic states are delocalized throughout the crystal, and filled and empty states are separated by band gap. The electronic states are called conduction band and hole states are called valence band. However, when size decreases, the density of states decreases from continuous state to discrete state confining the electrons and increasing the band gap, and changing the absorption and fluorescence wavelength, ionization potentials and electron affinities.[2] When the spatial dimensions constraining the wave function of electron are decreased one by one to the characteristic Bohr radius, the material changes from 3-D material to 2-D, 1-D and 0-D respectively. This changes the band gap.

These enhanced properties make nanomaterials applicable in various fields like medicine, catalysis, energy applications, data storage and computing and many others. Commonly studied nanomaterials include nanocrystals, nanotubes, nanowires, nanosized thin films, and nanosheets. These nanostructures are commonly fabricated by a top-down or bottom-up approach. In the top-down approach, bulk material is reduced to nanosize by photolithography and etching. This method has been used by engineers to create semiconductor computer chips. This may require large portion of materials as well as

excess waste and puts constraints on the dimensions that can be achieved and the number of structures that can be achieved. In the bottom-top approach, nanomaterials are synthesized by using building blocks of atomic or molecular components. Chemical vapor deposition (CVD), molecular beam epitaxy (MBE), and solution-liquid-solid (SLS) growth are some of the common ways to grow these nanostructures using bottom-up approach.

Products of bottom-up approaches can be zero dimensional materials such as quantum dots; one dimensional materials such as nanowires, nanotubes, and nanorods; and two dimensional material such as nanosheets. One dimensional material like nanowire, particularly semiconductor nanowires can be very important in electronics as they can be active devices, as well as help to interconnect devices to make integrated nanosystem. Therefore, this Thesis will focus on one dimensional semiconductor nanowires.

1.2 INTRODUCTION TO NANOWIRES

Nanowires are 1-D materials with confined electron waves in two spatial directions, and has diameter in nanoscale and length of few micrometers. Wagner and Ellis grew the first nanowires using vapor-liquid-solid (VLS) mechanism in 1964.[3] They grew Si nanowires using gold as a catalyst and called it silicon whiskers. After the discovery of carbon nanotubes,[4] semiconductor nanowires have been well investigated as a potential candidate in various electronic and optoelectronic devices due to their specific geometry and unique properties. These nanostructures have the potential to transform current microelectronics to nano-electronics in the near future due to the possibility of

high density of interconnections including between dissimilar materials. Commercial nanotube transistors have already been fabricated by IBM at present and are expected to replace various microelectronics by 2020. Reducing the size of these materials to the nanometer scale also allows for tuning the bulk electronic and optical properties. Among various semiconductor materials, elemental nanowires of group IVA like Si,[5 6] and Ge,[7 8] and nanowires of binary group III-V and II-VI compounds, like ZnS,[9 10] InAs,[11 12] CdS,[13 14] and GaN[15 16] have been extensively studied. Wide band gap II-VI materials like CdS and CdSe have been studied widely due to their potential in a variety of applications like electronic devices, photo emitting[14] and light detecting devices,[17] and solar cells.[18]

One advantage of nanowires is their length, diameter and composition can be controlled during growth. Normally, metal nanoparticles are used as catalyst to grow nanowires, and the diameter of these nanocrystals can control the diameter of nanowires. The growth time and amount of precursor can control the length of nanowires. Different precursor composition can change the composition of nanowires. The control of pressure and temperature is particularly important to get eutectic or sub-eutectic temperature, after which nanowire growth starts. Therefore, by controlling these parameters, similar nanowires can be produced each time containing similar electronic and optical properties. These morphology and crystallinity controlled nanowires are useful for electronic devices because of their high surface to volume ratio, characteristic length and width to absorb the light and transport the charges efficiently for photovoltaic applications, single crystal structure, and ability to be grown on different substrates.

The electronic and optical properties of semiconductor nanowires can be altered by synthesizing various heterostructures, by doping, and by using organic ligands to

terminate the surface. These heterostructures provide passivation, electrical isolation, or enhanced charge transfer, and internal field generation. The synthesis of heterostructures has been used in vertically aligned nanowire solar cells and horizontally aligned nanowire solar cells. Because of the promise of reduced material use and processing cost, strong light absorption, and improved charge separation mechanisms, nanowire solar cells are generating interest as an alternative to traditional silicon solar cells. The most common heterostructures are radial heterojunctions of core shell structure and axial heterojunctions. In a radial heterojunction, the charge separation will be efficient as the charge can be separated in a radial direction. Also, light will be trapped reducing the reflection of light and increasing the absorption.[19] Whereas, in axial heterojunction, there will be enhanced absorption of light because of light trapping, but loses the charge separation advantage.[19] The axial and radial heterostructures are normally achieved during the growth of nanowires.[20] A change in reactant supply during growth leads to axial and radial heterostructures depending on where the reactant is incorporated. When the reactants are incorporated in catalyst, axial heterostructures are formed, but when the reactants are incorporated throughout the nanowire surface, radial heterostructures are formed.

For CVD grown epitaxial Ge/Si core shell nanowires, it has been found that the band offset of Ge and Si produces an internal electric field which redistributes charge carriers and increases mobility of the nanowires.[21] Similarly, Peidong Yang's group synthesized CdS nanowires using VLS growth, and formed CdS/Cu_2S core-shell structure using cation exchange process.[18] His core-shell nanowires photovoltaic demonstrated 5.4% efficiency with higher open-circuit voltage and fill factor. Similarly axial heterostructures

containing combination of GaAs, GaP, InAs, InP, AlAs, Si, and Ge have also been synthesized.[22]

Another way to tune the electronic properties of nanowire is by incorporating impurities in nanowire crystal. This has been normally done during the growth of nanowires. Lieber's group has doped Si and Ge nanowires with boron and phosphorous to make p-type and n-type semiconductors.[23] They have also shown that high concentration dopants are possible in Si nanowires to have conductivity in the near metallic regime. It has also been shown that doping ZnTe nanowires with Cu increases the conductivity by three orders of magnitude.[24]Similarly people have also seen magnetism can be achieved in nanowires by doping. K L Wang and co-workers have shown that doping ZnO nanowires with Mn can produce ferromagnetism above room temperature.[25]

Similarly, another way to tune electronic properties of nanowires is by binding organic and elemental ligands on the nanowire surface. Because of the higher surface to volume ratio of nanowires, various surface states may be present on the nanowire, which act as trap states for light generated carriers, resulting in inefficient extraction of carriers. However, when the surface of nanowires are terminated with ligands, they can remove those surface states and provide surface passivation. It has been shown that halogen termination prevents oxidation in Ge nanowires and provides passivation.[26] Similarly, treating the InP nanowires with trioctylphosphine decreases non radiative recombination and increases the photoluminescence significantly.[27]

Compared to colloidal nanocrystals that are soluble in organic solvents, various challenges exist in modifying the surface of nanowires with ligands. Since, nanowires are larger compared to colloidal nanocrystals, they are not soluble. VLS grown nanowires are in the substrate, thus nanowires surface should be distinguished from the supporting substrate. Similarly, while making the device, nanowires are flat in the substrate, so the nanowire surface at the top only displays reactivity. One of the other challenges with nanowires is the technique to demonstrate ligand binding on the nanowire surface. Even though there exits many techniques that can detect ligands a lot of those techniques are hard to use because of insoluble nature of nanowires and the scale of nanowires grown.

NANOWIRE GROWTH

Various synthetic approaches have been used to grow nanowires including Vapor-Liquid-Solid (VLS) Growth,[9 5 28 29] Solution-Liquid-Solid (SLS) growth, [30] template based growth and solvothermal growth. However, much work has been focused on SLS and VLS growth because of the scalability of the growth, higher crystal quality, and capability of getting free standing nanowires.

1.2.1 VLS growth

VLS is the most commonly used method to grow nanowires. It is a high temperature growth which leads to single crystalline wires with little to no defects. The VLS growth mechanism was first discovered by Wagner and Ellis in 1964 at Bell Labs.[3] In this process, a metal nanocluster is used as a catalyst, and the catalyst is heated above the eutectic temperature in the presence of a vapor phase precursor to form a metal-

semiconductor alloy. With continuous feeding of the vapor phase precursor, the metal droplet supersaturates the eutectic and leads to the nucleation of nanowire. The metal - semiconductor interface acts as a growing interface, and nanowire growth takes place from bottom to top. Figure 1.1 shows the VLS mechanism of nanowire growth. In the growth of nanowire, there are two interfaces competing, the solid-liquid interface between the eutectic and nanowire, and the solid-vapor interface between nanowire and vapor phase precursors. If the precipitation takes place at the solid-liquid interface, it will result in VLS growth and nanowire will grow in axial direction. However, if dissociative adsorption takes place at the solid-gas interface, it will result in Vapor-Solid (VS) growth and the nanowire will thicken in radial direction. Either mechanism is possible during the growth of wire depending upon the growth conditions such as temperature, pressure, gas flow rate, and reactant species.

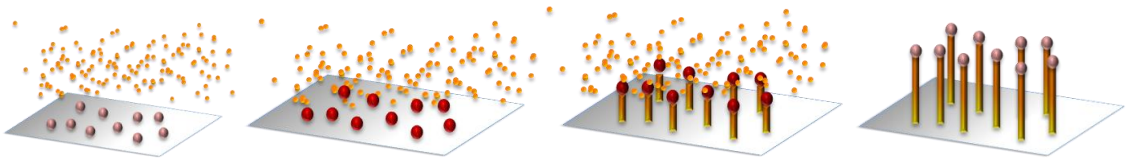

Figure 1.1 Schematic of VLS growth of nanowires.

1.2.1.1 VLS growth of CdS and CdSe nanowires

We constructed a vapor transport deposition system in our lab to grow CdS, CdSe and possibility of other nanowires. A schematic is shown in Figure 1.2. The source material for nanowire growth can be CdS powder, CdSe powder, or a single source

precursor for CVD. In a typical synthesis CdS or CdSe powder is deposited in an alumina boat in the upstream region, and a silicon substrate containing gold nanocrystals or gold film is placed in downstream side of quartz tube placed in tube furnace. The temperature and pressure inside the quartz tube can be controlled by the thermocouple of tube furnace and pressure controlled valve. Hydrogen and argon are used as carrier gases to transport precursor vapor to the substrate. The system has two more connections that can be used for more carrier gases or precursor gases. The system is sealed and connected to a vacuum pump to create oxygen free atmosphere and to provide an outlet for the processed gases.

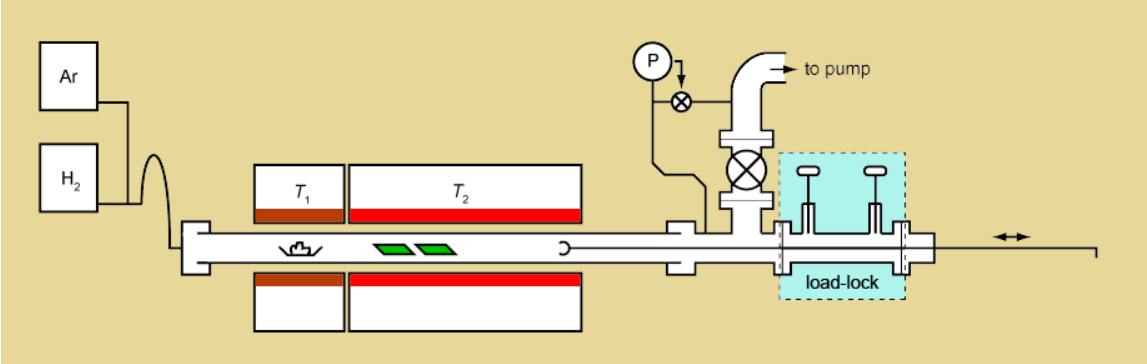

Figure 1.2 Schematic of chemical vapor deposition system

For synthesizing CdS nanowires, precursor temperature is kept around 780ºC and growth temperature around 550ºC. The pressure inside the quartz tube is maintained at 300 torr. 100 standard cubic feet per minute (SCCM) of Ar gas is used as carrier gas. After the temperature reaches to 780 ºC, the precursor boat is pushed to the center of furnace, and nanowires are grown for an hour. After growth, the system is cooled slowly to room temperature. The growth substrate is examined using dark field mode of optical microscopy, and electron microscope to examine their size and morphologies.

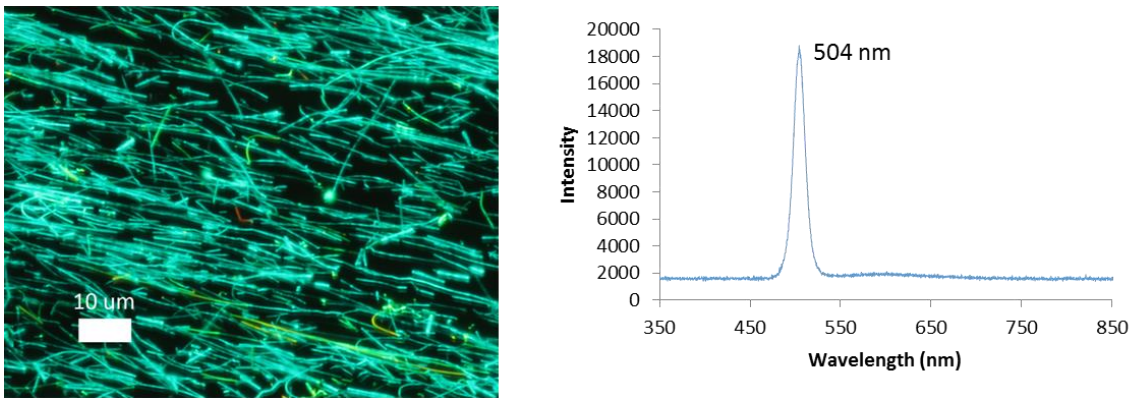

Figure 1.3 Fluorescence image and spectrum of CdS Nanowires transferred to new substrate from growth substrate

Figure 1.3 shows the fluorescence image and spectrum of CdS nanowires that are aligned horizontally on the Si substrate after mechanically transferring from growth substrate. The nanowires have strong fluorescence when excited at 365 nm excitation wavelength, showing a peak at around 504 nm which roughly corresponds to the band gap of CdS. There seems to be no or very little sub band gap emission. Figure 4 shows the microscopy images of CdS nanowires. Figure 1.4A is the dark field image of the nanowires. Because of the smaller diameter of nanowires than the wavelength of the light, it is very hard to see the wires through reflected light. Dark field provides a better mode to image nanowires as it collects the scattered lights. Figure 1.4B shows the SEM image of the nanowires. Nanowires are tens of microns long, and from the TEM image on Figure 4C, we can see nanowires are roughly 100 nm in diameter with smooth surfaces. High resolution TEM image suggests that nanowires have wurtzite crystal structure with (110) growth direction.

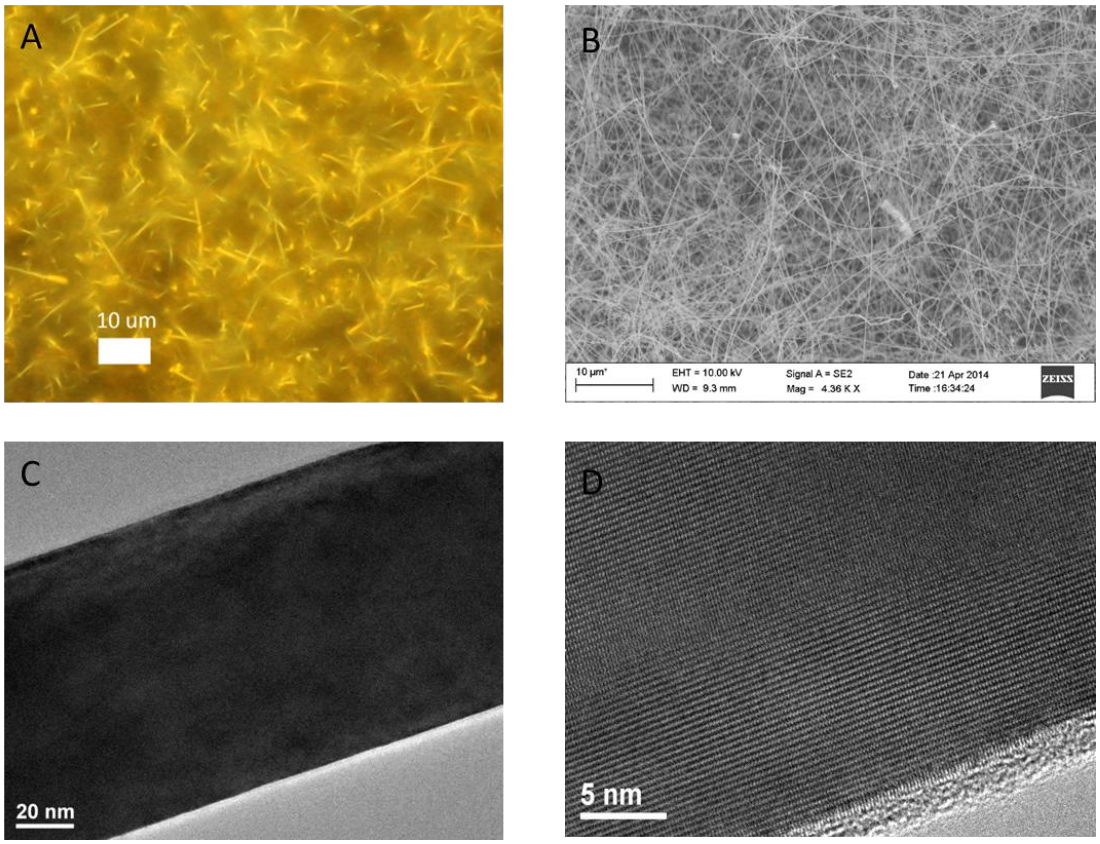

Figure 1.4 Dark field (A), SEM (B), TEM(C), and HR-TEM (D) images of CdS nanowires.

For synthesizing CdSe nanowires, Si substrate with 5nm gold deposited was used. The precursor temperature was held at 900°C, substrate temperature was held at around 400 °C, and the pressure was held at 300 torr. 25 SCCM of Ar and 55 SCCM of H_2 gas was used as the carrier gases. Nanowires were grown for an hour, after that the system was cooled to room temperature slowly. Figure 1.5 shows the fluorescence spectrum and SEM image of CdSe nanowires. An excitation wavelength of 510 nm reveals a fluorescence peak at around 712 nm representing band gap emission. There is no sub band gap emission indicating absence of emissive trap states. The SEM

images show the combinations of nanowires and nanobelts. The nanowire diameters are 100-500 nm, and are tens of microns long.

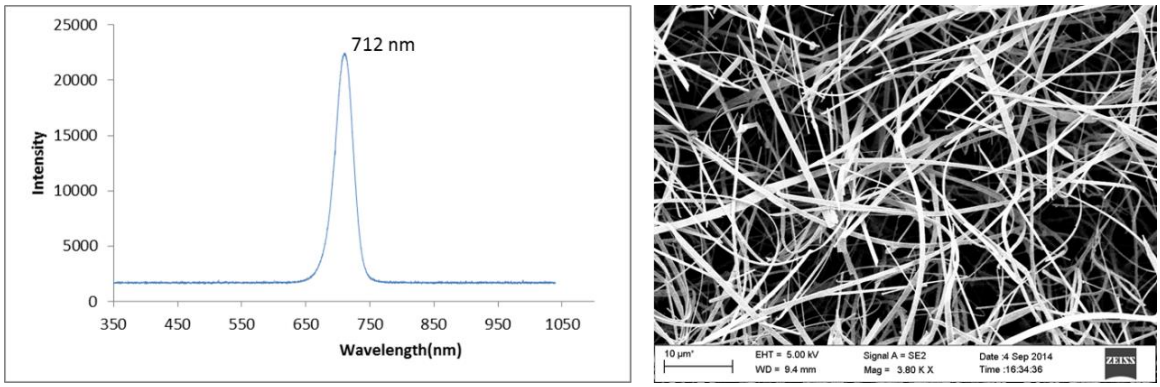

Figure 1.5: Fluorescence spectrum and SEM image of CdSe nanowires and nanobelts

1.2.2 SLS growth

SLS is relatively low temperature growth of semiconductor nanowires that can yield very small diameter nanowires with controlled surface ligation. This method of nanowire growth was first discovered by Buhro's group in 1995.[31] It is very similar to VLS growth of nanowires, except for low growth temperature (<400 ºC) and solution phase precursor. Normally low melting metal like Bi, Sn, In and Ga are used as a catalyst for the growth.[32] In this process, after heating, the solution phase precursor thermolyze yielding elements of the desired semiconductor. These elements of desired semiconductor solubilize with molten catalyst droplets. After saturation, nucleation event takes place in the interface of liquid catalyst droplet and solution which initiates nanowire growth. With addition of precursor to nucleated seed, nanowires start growing from bottom to top. Figure 1.6 illustrates the SLS growth mechanism of nanowires.

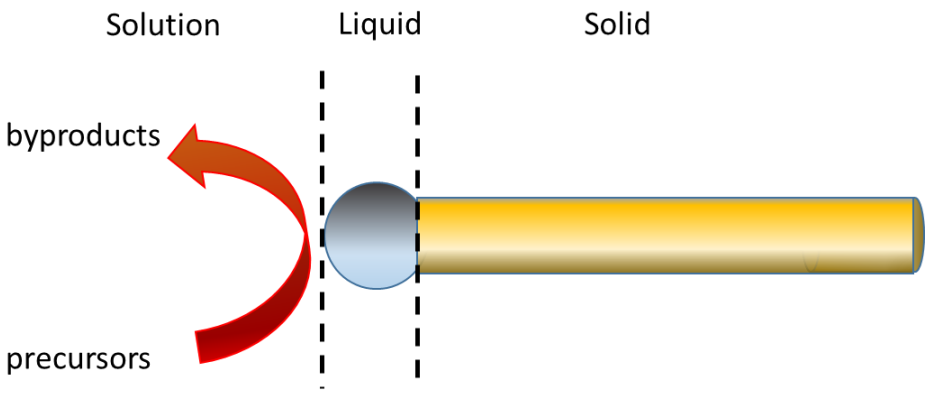

Figure 1.6: Schematic of SLS growth mechanism of nanowire

The diameter of catalyst nanoparticles closely control the diameter of the nanowires. In this process surface of nanowires are attached with organic surfactants that reduce lateral growth of nanowires yielding very small diameter, as well as suppresses oxidation in the surface. The yield of SLS growth can be higher, and the nanowires can be suspended in a variety of solvents. The surface chemistry developed for colloidal nanocrystals may be more directly applicable to these nanowires than to VLS products as they have native ligands that provide steric stabilization and, in principle, a known starting point for surface chemistry. Even though people have achieved crystalline nanowires from SLS growth, being a low temperature growth it is more prone to various crystalline defects.

The setup for typical SLS synthesis of nanowires is similar to nanocrystals. A typical set up to synthesize nanowires is shown in figure 1.7. Normally a metal salt or oxide like CdO is used as metal precursor, and trioctylphosphine sulfide (TOPS), or trioctylphosphine selenide (TOPSe) is used as S or Se precursor. The solvents for the

synthesis are normally high boiling coordinating solvents like trioctylphosphine oxide (TOPO), or non-coordinating solvents like octadecene. With non-coordinating solvents, there are ligands added or precursor byproducts behave as ligands. Low boiling point Bi nanoparticle is generally used as a catalyst for nanowire growth.

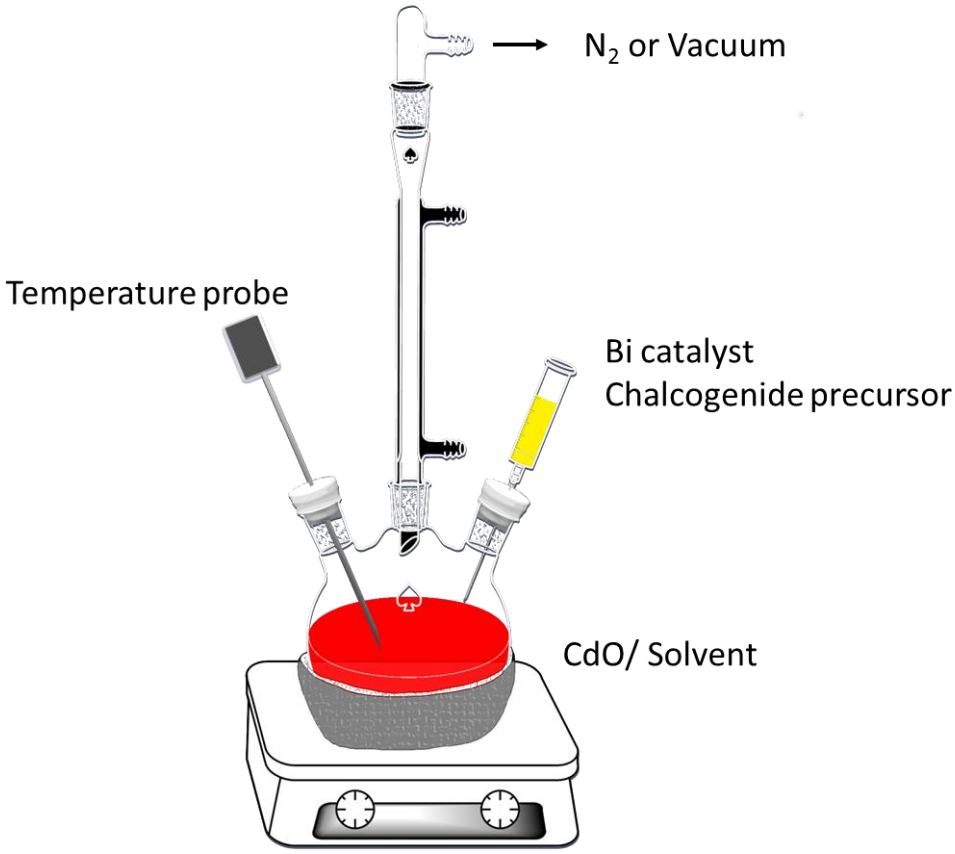

Figure 1.7: Typical set up to synthesize nanowires using SLS process

Before synthesizing CdS and CdSe nanowires, Bi nanoparticles were synthesized following the procedure used by slight modification of Alf Mews' group.[33] Bismuth chloride ($BiCl_3$) was dissolved in bis-phenyl ether slowly until completely dissolved. After dissolving bismuth chloride, bismuth chloride was reduced to obtain bismuth nanoparticles by adding TOP slowly with continuous stirring inside the glove box. In order to stabilize bismuth nanoparticles, oleylamine was added in excess (10X by mole of bismuth). The solution was stirred for 30 minutes until brown, and was used to grow nanowires.

CdSe nanowire was grown using Alf Mews' method.[33] In a round bottom flask CdO, TOPO and oleic acid were combined. The mixture was dried and degassed for 30 minutes at 100 ºC. After 30 minutes, the system was purged with nitrogen gas, and heated to 300 ºC. When the temperature stabilizes, Bi nanoparticle and TOPSe was injected. After 1 minute of injection, the system was allowed to cool to room temperature. In order to prevent solidifying of TOPO, toluene was injected at around 100 ºC. Nanowires were precipitated using excess of butanol. Excess ligands were removed by precipitation and re-dissolution of nanowires using butanol and toluene. Lastly, the nanowires were suspended in toluene. Figure 1.8 shows an SEM image of CdSe nanowires grown using SLS method. A drop of toluene containing nanowires was cast on a Si substrate and observed through microscopy after the solvent was evaporated. The nanowires are around 40-50 nm, and Bi metal is visible in the tip of nanowires confirming catalyst assisted growth.

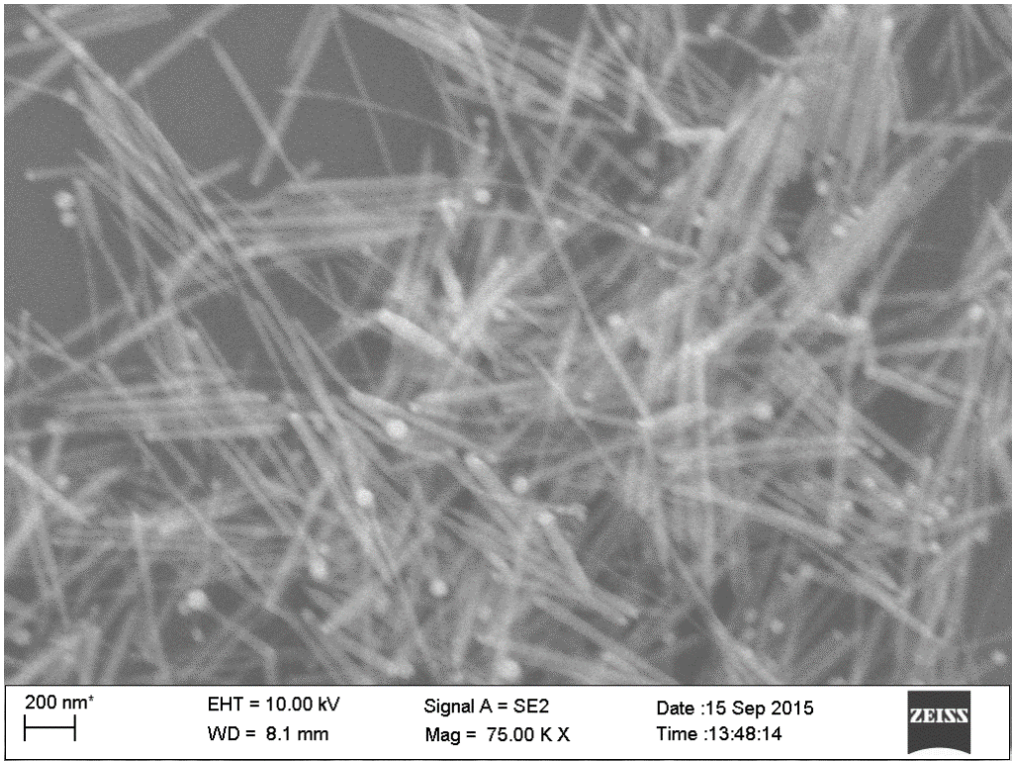

Figure 1.8: SEM image of CdSe nanowire synthesized using SLS growth

CdS nanowires were grown using the modification of the Kuno's process.[30] In a round bottom flask, CdO, dodecylamine (DDA), TOPO, and oleic acid were combined. The system was dried and degassed for an hour at 80ºC. After that the system was purged with nitrogen gas and the system was heated to 315ºC. When the temperature had stabilized, a solution of bismuth nanoparticle and TOPS was injected. The nanowires were allowed to grow for 2 minutes, and then the system was allowed to cool to room temperature. In order to prevent solidification of TOPO, toluene was added during cooling. The nanowires were extracted using excess of methanol and purified by precipitation and re-dissolution of nanowires using methanol and chloroform, resulting in wires dispersed in chloroform. Figure 1.9 shows the SEM image CdS nanowire grown

using SLS process. A drop of solvent containing nanowires was dropped on a Si substrate, and nanowires were observed through SEM after the solvent was evaporated.

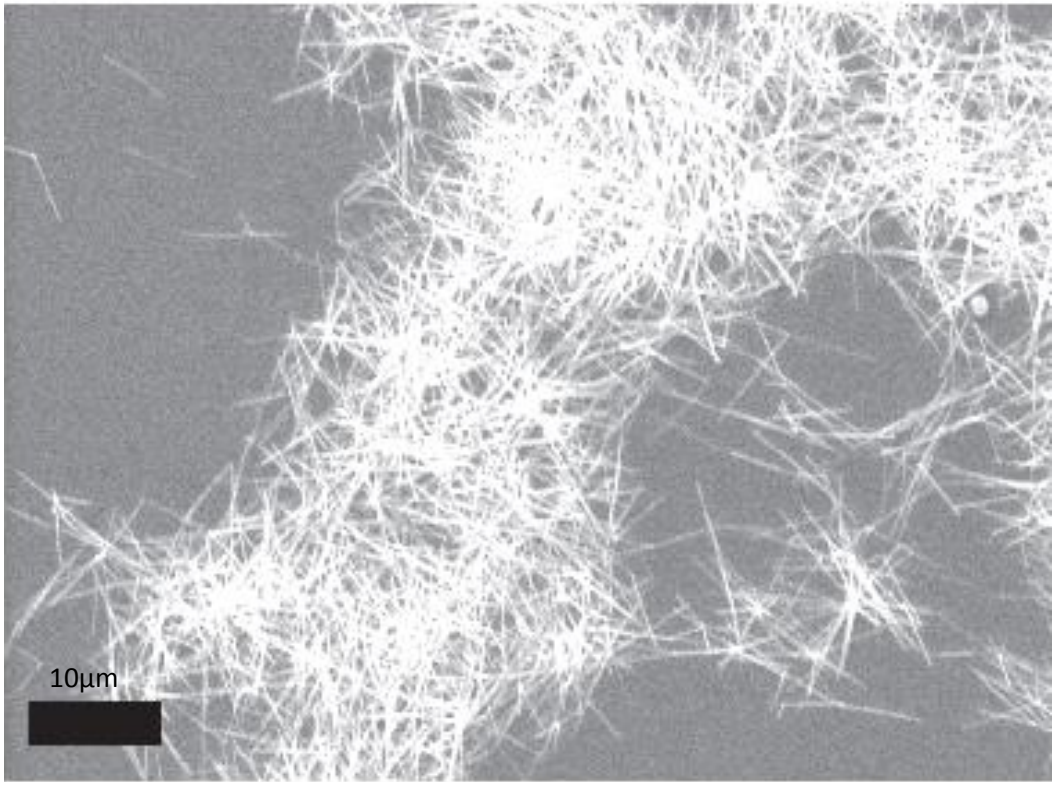

Figure 1.9: SEM image of CdS nanowires synthesized using SLS growth

1.3 CONCLUSION

Our lab was successfully able to synthesize CdS and CdSe nanowires using VLS and SLS growth mechanism. The VLS grown nanowires have larger diameter, highly fluorescence, high crystallinity, and can be used to study the charge transports. The SLS growth nanowires have very low photoluminescence with some organic ligands. These wires can be a model material to imitate the surface chemistry studied in colloidal nanocrystals.

1.4 THESIS OVERVIEW

This thesis will be focused on the surface chemistry of nanowires and their consequences on the electronic properties. The first chapter introduced the nanowires and its potential applications on various opto-electronic devices. It also explained various different mechanism to grow different composition of nanowires. The nanowire growth process used in our lab has been explained, and the the results have been shown. The morphology, fluorescence spectrum, and crystal structure of as grown nanowires has been shown.

The second chapter of the thesis will focus on the demonstration of ligand binding on the nanowire surfaces using fluorescence microscopy, and potential of this measurement to study the kinetics of ligand binding on the nanowire surfaces. The ternary copolymer used in this experiment has three important functional groups: multiple imidazole group to bind to the native surface of CdS nanowires, PEG group to provide water solubility, and primary amine group to attach a dye load, here a fluorescence dye. The attachment of these ternanry copolymer has been demonstrated using fluorescence microscopy using appropriate emission and excitement filters. The later part of the chapter talks about the kinetics of ligand binding on the nanowire surface using fluorescence microscopy. The fabrication of microfluidic channel to study the kinetics of binding as well experimental procedure and the obtained kinetics data will be explored.

The third chapter will focus on surface chemistry of nanowires and their consequences in their optical and electronic properties. Photoluminescence data will be presented before and after ligand binding on the nanowire surfaces. This chapter will also

focus on the nanofabrication including all the steps to get nanowire device. The electronic properties of nanowires will be explored using dark and photocurrent measurements, and persistent photocurrent will be discussed.

The fourth chapter will explore the transport properties of higher dimensional and organic microfibers. The transport properties of as synthesized and iodine doped microfibers will be discussed. The device fabrication steps to make those organic microfiber device would be presented and details of doping experiment will be discussed.

References

(1) *Nat. Nanotechnol.* **2009**, *4* (12), 781–781.

(2) Roduner, E. *Chem. Soc. Rev.* **2006**, *35* (7), 583–592.

(3) Wagner, R. S.; Ellis, W. C. *Appl. Phys. Lett.* **1964**, *4* (5), 89–90.

(4) Iijima, S. *Nature* **1991**, *354* (6348), 56–58.

(5) Wu, Y.; Cui, Y.; Huynh, L.; Barrelet, C. J.; Bell, D. C.; Lieber, C. M. *Nano Lett.* **2004**, *4* (3), 433–436.

(6) Cui, Y.; Lauhon, L. J.; Gudiksen, M. S.; Wang, J.; Lieber, C. M. *Appl. Phys. Lett.* **2001**, *78* (15), 2214–2216.

(7) Wu, Y.; Yang, P. *Chem. Mater.* **2000**, *12* (3), 605–607.

(8) Gu, G.; Burghard, M.; Kim, G. T.; Düsberg, G. S.; Chiu, P. W.; Krstic, V.; Roth, S.; Han, W. Q. *J. Appl. Phys.* **2001**, *90* (11), 5747–5751.

(9) Barrelet, C. J.; Wu, Y.; Bell, D. C.; Lieber, C. M. *J. Am. Chem. Soc.* **2003**, *125* (38), 11498–11499.

(10) Wang, Y.; Zhang, L.; Liang, C.; Wang, G.; Peng, X. *Chem. Phys. Lett.* **2002**, *357* (3–4), 314–318.

(11) Hang, Q.; Wang, F.; Carpenter, P. D.; Zemlyanov, D.; Zakharov, D.; Stach, E. A.; Buhro, W. E.; Janes, D. B. *Nano Lett.* **2008**, *8* (1), 49–55.

(12) Ford, A. C.; Ho, J. C.; Chueh, Y.-L.; Tseng, Y.-C.; Fan, Z.; Guo, J.; Bokor, J.; Javey, A. *Nano Lett.* **2009**, *9* (1), 360–365.

(13) Ye, C.; Meng, G.; Wang, Y.; Jiang, Z.; Zhang, L. *J. Phys. Chem. B* **2002**, *106* (40), 10338–10341.

(14) Duan, X.; Huang, Y.; Agarwal, R.; Lieber, C. M. *Nature* **2003**, *421* (6920), 241–245.

(15) Hersee, S. D.; Sun, X.; Wang, X. *Nano Lett.* **2006**, *6* (8), 1808–1811.

(16) Chen, X.; Xu, J.; Wang, R. m.; Yu, D. *Adv. Mater.* **2003**, *15* (5), 419–421.

(17) Hayden, O.; Agarwal, R.; Lieber, C. M. *Nat. Mater.* **2006**, *5* (5), 352–356.

(18) Tang, J.; Huo, Z.; Brittman, S.; Gao, H.; Yang, P. *Nat. Nanotechnol.* **2011**, *6* (9), 568–572.

(19) Garnett, E. C.; Brongersma, M. L.; Cui, Y.; McGehee, M. D. *Annu. Rev. Mater. Res.* **2011**, *41* (1), 269–295.

(20) Lauhon, L. J.; Gudiksen, M. S.; Lieber, C. M. *Philos. Transact. A Math. Phys. Eng. Sci.* **2004**, *362* (1819), 1247–1260.

(21) Lauhon, L. J.; Gudiksen, M. S.; Wang, D.; Lieber, C. M. *Nature* **2002**, *420* (6911), 57–61.

(22) Dick, K. A.; Kodambaka, S.; Reuter, M. C.; Deppert, K.; Samuelson, L.; Seifert, W.; Wallenberg, L. R.; Ross, F. M. *Nano Lett.* **2007**, *7* (6), 1817–1822.

(23) Cui, Y.; Duan, X.; Hu, J.; Lieber, C. M. *J. Phys. Chem. B* **2000**, *104* (22), 5213–5216.

(24) Huo, H. B.; Dai, L.; Liu, C.; You, L. P.; Yang, W. Q.; Ma, R. M.; Ran, G. Z.; Qin, G. G. *Nanotechnology* **2006**, *17* (24), 5912.

(25) Chang, L.-T.; Wang, C.-Y.; Tang, J.; Nie, T.; Jiang, W.; Chu, C.-P.; Arafin, S.; He, L.; Afsal, M.; Chen, L.-J.; Wang, K. L. *Nano Lett.* **2014**, *14* (4), 1823–1829.

(26) Adhikari, H.; McIntyre, P. C.; Sun, S.; Pianetta, P.; Chidsey, C. E. D. *Appl. Phys. Lett.* **2005**, *87* (26), 263109.

(27) van Vugt, L. K.; Veen, S. J.; Bakkers, E. P. A. M.; Roest, A. L.; Vanmaekelbergh, D. *J. Am. Chem. Soc.* **2005**, *127* (35), 12357–12362.

(28) Gu, Y.; Romankiewicz, J. P.; David, J. K.; Lensch, J. L.; Lauhon, L. J. *Nano Lett.* **2006**, *6* (5), 948–952.

(29) Gu, Y.; Romankiewicz, J. P.; David, J. K.; Lensch, J. L.; Lauhon, L. J.; Kwak, E.-S.; Odom, T. W. *J. Vac. Sci. Technol. B* **2006**, *24* (4), 2172–2177.

(30) Puthussery, J.; Lan, A.; Kosel, T. H.; Kuno, M. *ACS Nano* **2008**, *2* (2), 357–367.

(31) Trentler, T. J.; Hickman, K. M.; Goel, S. C.; Viano, A. M.; Gibbons, P. C.; Buhro, W. E. *Science* **1995**, *270* (5243), 1791–1794.

(32) Kuno, M. *Phys. Chem. Chem. Phys.* **2008**, *10* (5), 620–639.

(33) Li, Z.; Kornowski, A.; Myalitsin, A.; Mews, A. *Small* **2008**, *4* (10), 1698–1702.

CHAPTER 2

DEMONSTRATION AND KINETIC STUDY OF LIGAND BINDING ON SINGLE CDS NWS

2.1 INTRODUCTION

When the bulk material is reduced to nanomaterial, the fraction of atoms at surface increases giving higher surface to volume ratio. This causes lower coordination of surface atoms, and unsatisfied bonds. These unsatisfied atoms form the surface states which act as trap sites for photogenerated excitons, which may cause non radiative recombination, or inefficient charge extraction. This interaction of excitons with surface states is the main limitation for photoluminescence[1], which is an indirect measurement of surface recombination, which affects optoelectronic devices. Binding the ligands on the nanomaterial surfaces have been shown to be effective way to remove these surface states. When a ligand binds to the surface, the HOMO and LUMO of the ligand interact with the surface state to form hybridize state. This hybridize state depends on the position of HOMO and LUMO and can remove the trap state[2] or induce a trap state[3] in the semiconductor surface. Therefore, proper choice of ligand is necessary to remove the surface state present in the semiconductor nanowire surfaces.

Since the optical and electronic properties of nanowires are strongly affected by the surface[4], much interest has been given to modify the surface of nanowires by binding

molecular ligands to the surface to achieve desired optical and electronic properties.[5] The molecular ligands that bind to the surface influence the surface state density and electrostatic charge density present in the surface of a nanowire. The passivation of surface state helps in efficient separation of charge that can increase the efficiency of electronic devices like photovoltaics. Growing conformal inorganic layers on the surface of nanowires to get core-shell homo[6] and hetero-structures[7] have also shown effective increase in photoluminescence quantum yield. This core-shell structure can also help to increase the efficiency of charge collection by reducing the distance travelled by minority charge carrier[8] in device structures where carrier collection takes place in shorter radial direction rather than longer axial direction.[9]

A large number of studies have been done to examine the consequences of surface modification in case of colloidal semiconductor nanocrystals. These nanocrystals as synthesized have a native ligand. The identity of the ligands can be determined by various techniques such as NMR. However, these ligands are often exchanged to get the desired electronic and optical properties. It has been shown in Greytak's group that introducing TOP to oleate terminated CdSe/CdZnS increases the photoluminescence significantly by reducing non radiative recombination.[10] This is attributed to binding of TOP to vacant sites. Similarly, Owen's group has shown that exchanging neutral phosphine ligand with neutral amine ligand increases the photoluminescence of CdSe quantum dots significantly.[11] Murray group has shown that replacing the bulky organic layers with sulfide ligand increases the charge transfer in CdSe QD sensitized solar cells by removing insulating organic barrier.[12] Similarly, Weiss group has demonstrated ligand exchange on CdSe QDS with para-substituted anilines. Her group has shown that replacing the original ligands with

para substituted ligands decreases the photoluminescence.[13] Out of many ligands, most commonly studied ligands are anionic ligands that bind to cation rich surface, like halide[11], phosphonate[14], carboxylate[15], and dative or neutral ligands that bind to Lewis acid surfaces, like amine[11], thiol[14] and alkyl phosphonic acid[16].

Despite of much progress in the studying the surface chemistry of colloidal nanocrystals, very less work has been done in nanowires. Holmes group has been able to terminate the surface of Germanium NWs with Halogen, and have demonstrated using XPS that these halogen can passivate the surface and prevent oxidation in the surface of NWS.[17] There are many examples of using ligands to bind on the Si nanowire substrate, but results for non-Si are scarce. Lewis group has been able to terminate the Si surfaces with halides and methyl group and has been able to calculate the extent of band bending using X ray Photoelectron spectroscopy (XPS).[18] Similarly, Buhro group passivated InAs NW surfaces with 1-octadecanthiol.[19] They found an increase in mobility and reduction in subthreshold slope is associated with reduction of InAs surface state due to bonding of thiol molecule. Similarly Kagan's group has shown that by treating CdSe nanowires with cadmium acetate, sodium selenide and sodium sulfide gives cadmium rich, selenium rich, and sulfide rich surfaces[20]. These nanowires with different surfaces have been demonstrated to have different electronic properties.

The main goal of this project is to use the surface chemistry performed in colloidal nanocrystals, and apply these concepts to higher dimensional materials like nanowires. This technique can be extended to various other nanowires with different compositions, as well as to probe the interactions of various unlabeled molecular ligands on nanowire surfaces. We first were able to demonstrate ligand binding on CdS

nanowires by using fluorescence microscopy. Since a single nanowire can be resolved through fluorescence microscopy, this method can be extended to study the kinetics of ligand binding on the nanowire surfaces. Kinetic study of ligand binding can be very important to study the surface chemistry as it provides information about the nature of the nanowire surfaces, and association and dissociation rate constants of binding.

To investigate ligands binding on CdS nanowire surfaces, we chose two examples of imidazole bearing macromolecular ligands that could be easily labeled with fluorescent dyes. Macromolecules are particularly interesting as they allow unbound dye to be easily removed by using proper centrifuge filters. The first macromolecules used is Grx4 protein which is tagged with poly histidine group and has 3 cysteine and 7 lysine residue. The other macromolecule used is terpolymer. This ternary copolymer was synthesized by RAFT polymerization technique using imidazole monomers. These terpolymers are incorporated with 3 different functional groups for three different functions: multiple imidazoles for attachment with CdS surface, PEG chains for solubility in aqueous media, and primary amines for attachment of fluorescence dye.

2.2 DEMONSTRATION OF FLUORESCENTLY LABELED LIGAND BINDING TO NANOWIRE SURFACES

Polymeric ligands with different functional groups have been recently used to tune the properties of the CdS surfaces as well as to disperse nanocrystals in polymer matrix.[21] Polymeric imidazole has been shown to be a strong binder to cadmium chalcogenide nanocrystal surfaces.[22,23] Binding of imidazole to CdS and similar surfaces is believed to be driven by a metal affinity interaction between imidazole nitrogen and

surface cadmium atoms[24]. We sought to determine whether polymeric imidazole ligands could be used to functionalize the native surface of vapor-deposited CdS NWs. The development of deliberate polymer strategies to functionalize CdS NWs has not been reported, nor are we aware of previous examples in which fluorescently labeled ligands have been employed to directly probe ligand binding to compound semiconductor NWs. The ternary copolymer used in this experiment has three important functional group: multiple imidazole group to bind to the native surface of CdS nanowires, PEG group to provide water solubility, and primary amine group to attach a dye load, here a fluorescence dye. This work has been published in Polymer Chemistry, 2015(DOI: 10.1039/C5PY00685F).

2.2.1 Conjugation of terpolymer with rhodamine dye

Commercially available 5-(and-6)-Carboxy-X-Rhodamine succinimidyl ester (5 (6)-ROX, SE) was dissolved in dry DMSO to make a stock solution of dye. A known amount of amine functional polymer was dissolved in aqueous 0.1M $NaHCO_3$ solution. 10 equivalents of dye (per polymer chain) were mixed with polymer solution and were continuously vortexed for 2 hours to achieve polymer-dye conjugation. Excess dye was removed by dialysis with bicarbonate buffer using 10K MW cutoff centrifugal filters; centrifugal dialysis was continued until eluent was clear. The total concentration of dye in the final product was calculated using UV-visible absorption spectroscopy. Assuming no polymer was lost during dialysis and transferring, the average number of dyes per polymer chain was calculated to be 0.25; this number therefore represents a lower bound. Figure 2.1 shows the structure of ternanry polymer (A), amine reactive dye (B), and UV-Vis spectra of dye and dye labeled polymer(C).

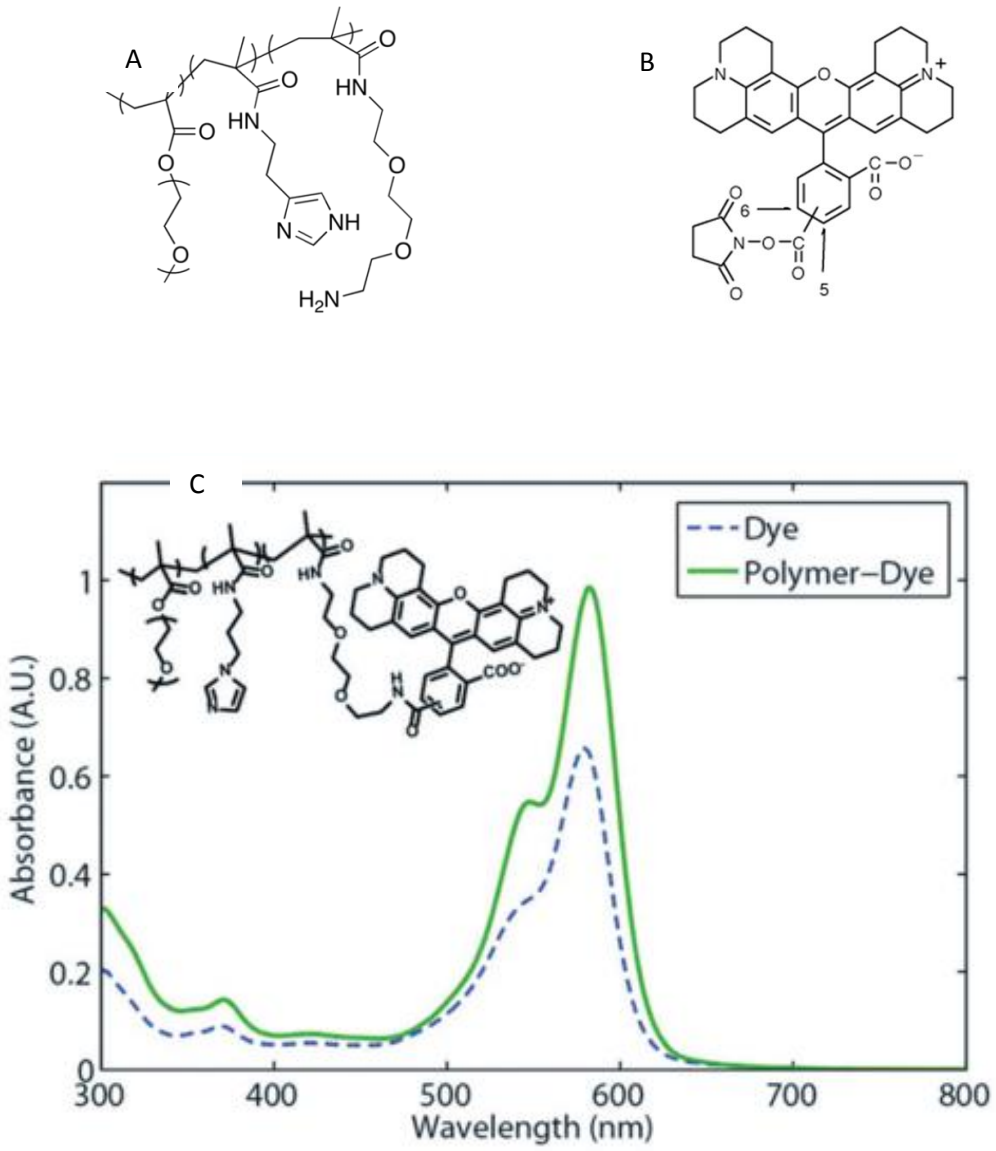

Figure 2.1 A. Structure of polymer, B. Structure of dye, C. UV-Vis of dye (blue dashed line), and dye labeled polymer (green).

2.2.2 Treatment of nanowires with polymer dye conjugate solution

CdS NWs on the growth substrate were treated with dye-labeled polymer solution (total dye concentration: 5 μM) for 2 hours. After 2 hours, the substrate was thoroughly rinsed with aqueous $NaHCO_3$ solution. As a control, a similar substrate with CdS NWs

was treated with 5 µM free dye solution for 2 hours and similarly rinsed. NWs were then dispersed in aqueous solution by sonication; a drop of this suspension was placed on a microscope glass slide, covered with a glass cover slip, and observed through the microscope. Figure 2.2 shows the schematic of dye labeled polymer binding on CdS NW surface.

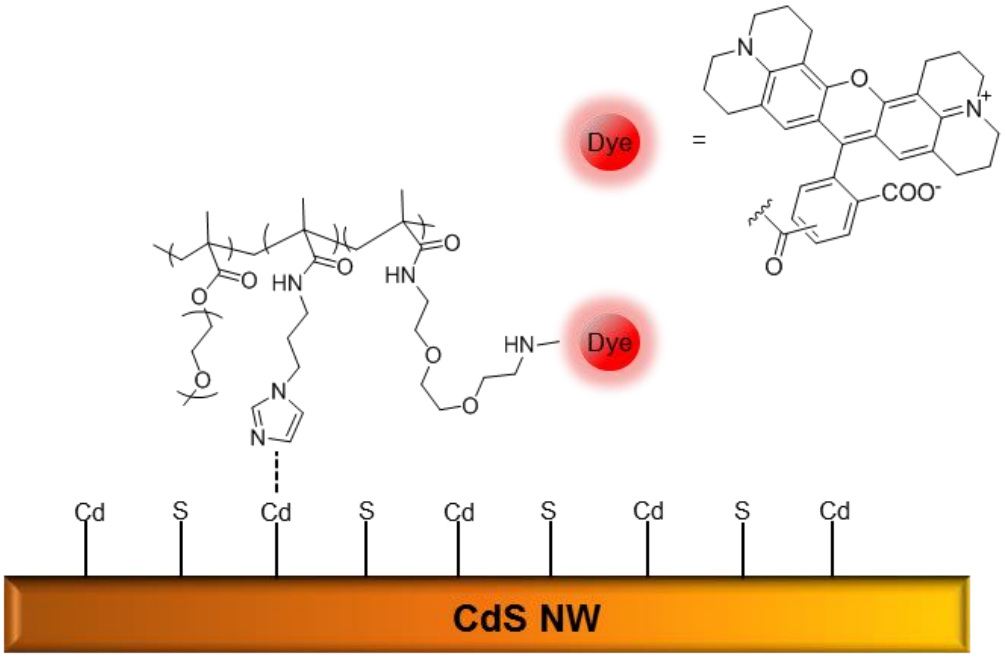

Figure 2.2 Schematic of dye labeled polymer attaching to the nanowire surfaces

2.2.3 Fluorescent microscopy results

CdS nanowires were synthesized by a physical vapor transport method. The growth substrate was examined with field-emission scanning electron microscopy and was found to contain primarily NWs (40-200nm in diameter) as well as some nanobelts with widths up to a micron (Figure 2.3). UV-visible absorption

spectroscopy of the free dye and dye labeled polymer revealed little change in the peak position or line shape (Figure 2.1(C)). Based on the absorbance of the purified polymer-dye sample measured at a known dilution, and the published extinction coefficient of the ROX, SE dye, an average dye-per-polymer ratio of 0.25 was calculated. In order to confirm the attachment of the dye-functionalized polymer to the NW surfaces, fluorescence microscopy was used to analyze the CdS NWs treated with the dye functionalized polymer and with the free rhodamine dye. Dark field microscopy was used to locate single nanowires, while the fluorescence image, which is sensitive only to dye emission, is used to identify localization of the dye labeled polymer to the NW surfaces.

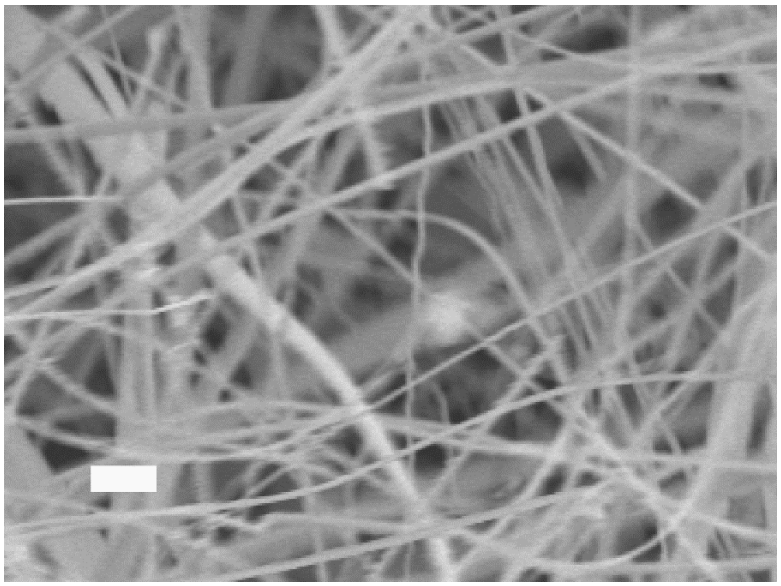

Figure 2.3 SEM image of CdS nanowire sample supported on Si growth substrate. Scalebar, 1 μm.

Figure 2.4 shows representative darkfield and fluorescence images of a NW treated with the dye labeled terpolymer. The NW is clearly visible in darkfield mode

owing to high dielectric contrast with the surrounding medium. The NW is also clearly visible in fluorescence mode when illuminated with sub-bandgap light at the dye excitation wavelength. The prominent fluorescence mode signal demonstrates clearly the presence of the dye on the NW surface. Figure 2.5 shows a representative image from the control experiment in which NWs were exposed to free dye. In the fluorescence image, at the location of the NW, the signal cannot be distinguished from background.

A particular advantage of NWs as a target for fluorescence measurement of ligand binding to inorganic surfaces is their quasi one-dimensional shape; the fluorescence intensity profile measured orthogonal to the NW should vary slowly with respect to translation along the NW axis. The dark field and fluorescence intensity traces shown in Figs. 2.4 and 2.5 represent profiles averaged along the NW axis over a width represented by the red boxes in the images; this analysis improves the signal to noise ratio and helps in distinguishing the NW intensity signal from background. The absence of a fluorescence signal from the dye in the control case suggests that the free dye is incapable of complexing with the NW surface under the experimental conditions.

Comparison of the dye-labeled polymer treatment and the control experiment clearly identifies the ability of the terpolymer ligand units to simultaneously bind to the NW surface and the dye payload. These experiments confirm the hypothesis that a terpolymer with three discrete functionalities is capable of binding to unmodified CdS nanowire surfaces, and paves the path for new opportunities in the optoelectronic field.

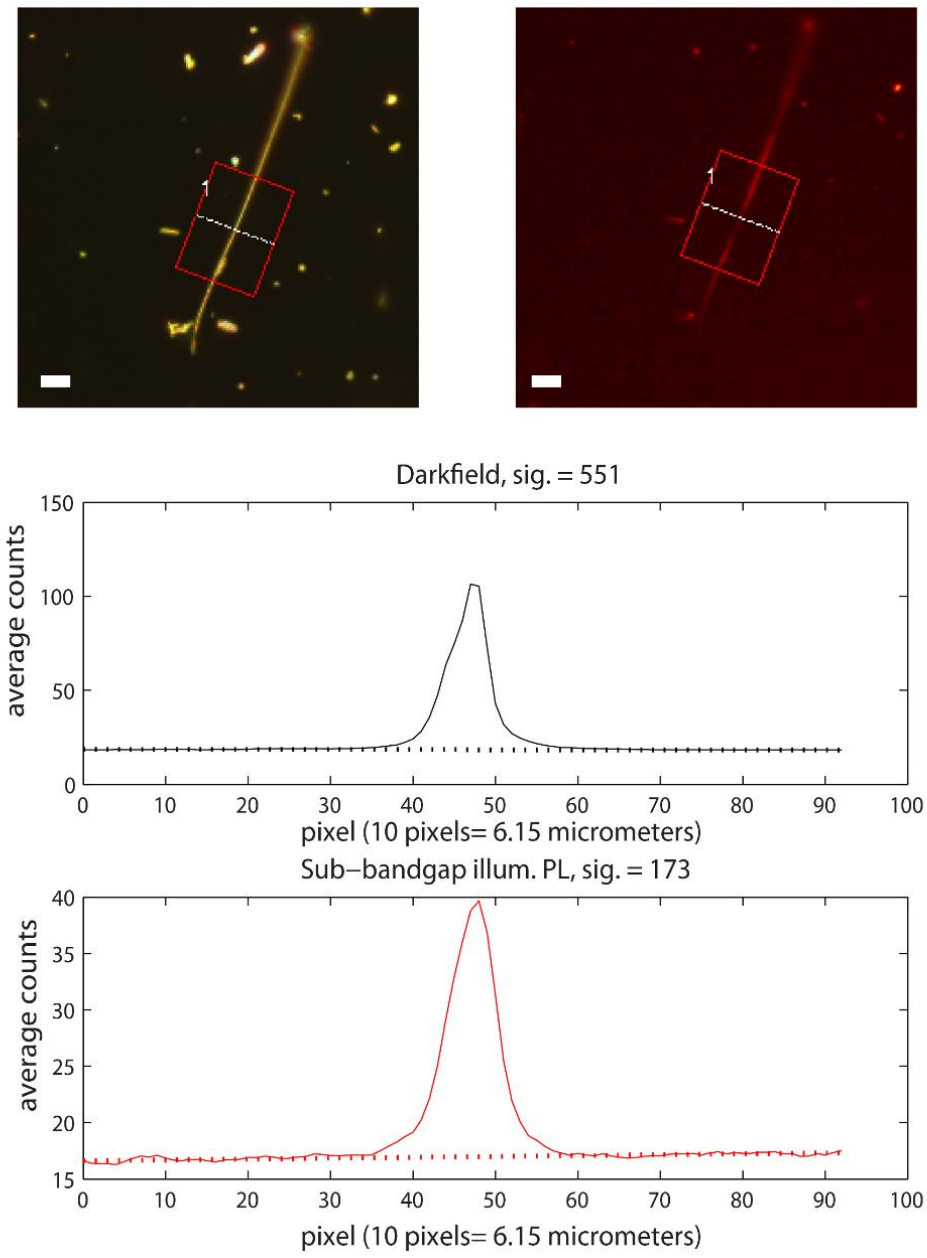

Figure 2.4 Optical micrographs of a representative CdS NW treated with dye-labeled terpolymer ligand. (Top left) True color image of NW in dark field mode. (Top right) False color image of the same location in fluorescence mode. Scale bars 10 μm. Dark field and fluorescence intensity profiles centered on the dashed lines marked "1" in the images are shown below.

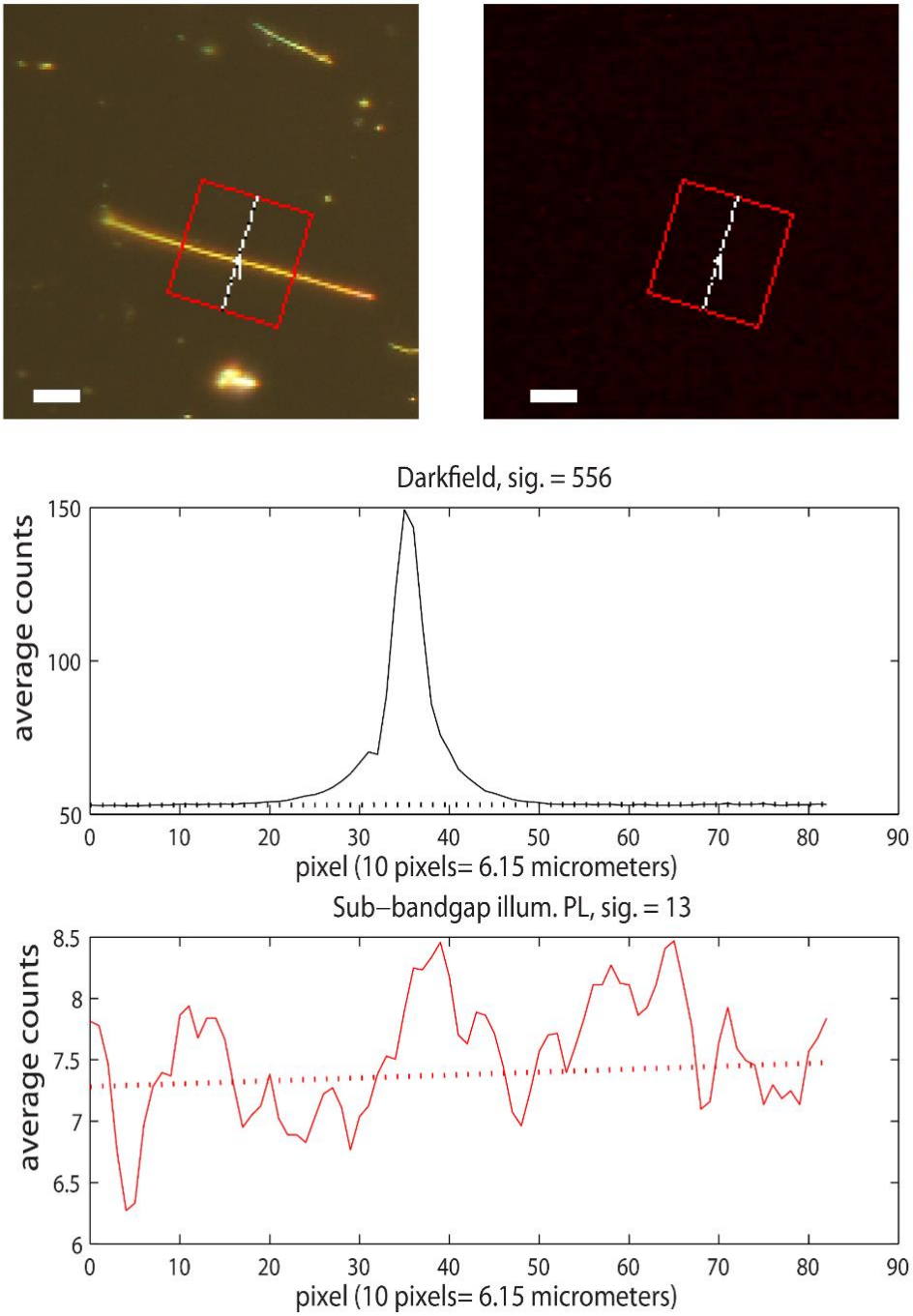

Figure 2.5 Optical micrographs of a representative CdS NW treated with free carboxyrhodamine dye. (Top Left) True color image of NW in dark field mode. (Top Right) False color image of the same location in fluorescence mode. Scale bars 10 μm. Dark field and fluorescence intensity profiles centered on the dashed lines marked "1" in the images are shown below;

2.3 KINETIC STUDY OF LIGAND BINDING

In-situ measurement of the binding and releasing of fluorescently labeled ligands on the immobilized semiconductor nanowire can help to understand the interaction between organic ligands to nanowire surfaces, which will be eventually useful to understand how these surface chemistry will change the electronic properties of nanowires. Poly-His tagged protein was chosen as a starting ligand as it has been shown to bind to the metal sulfide nanocrystal surfaces.[24] A dye labeled ligand and an aqueous buffer solution will be alternately flown over immobilized nanowires, and the corresponding fluorescence signal will be monitored overtime. The fluorescence dye will be selectively excited by choosing the light intensity below the band gap of NWs. The fluorescence intensity collected will be proportional to the concentration of dye labeled ligand.

In order to calculate the adsorption and desorption rate constant, first order bi-molecular reaction kinetic model is used.

$$B + L \rightarrow BL$$

Where B is available binding site, L is fluorescently labeled ligand, and BL is occupied binding site. During continuous flow of protein solution, concentration of bound ligand exponentially increases with time until the concentration of the ligand adsorbed on the surfaces reaches the maximum point (equilibrium). This on-phase can be used to calculate adsorption rate constant (k_{on}) and desorption rate constant (k_{off}). In the on-phase, the relationship between the concentrations of the ligand bound to the surfaces of the NW at a particular time, t ($[BL]_t$) and at the equilibrium ($[BL]_e$) can be written as

$$[BL]_t = [BL]_e (1 - e^{-k_{app}*t})$$

Where, $k_{app} = k_{on}[L] + k_{off}$

While washing the NWs with clean solution, the number of bound sites will decays exponentially which can give k_{off}. After repeating the experiments with different concentrations of ligands, k_{on} and k_{off} can be extracted. After calculating k_{on} and k_{off}, binding constant K_a can be calculated from the equation:

$$K_a = \frac{k_{on}}{k_{off}}$$

2.3.1 Microfluidic device fabrication

In order to perform in-situ study of ligand binding on nanowire surface, microfluidic device was fabricated. The device consists of polydimethyl siloxane (PDMS) elastomer stamp consisting a channel that was created using SU-8 epoxy master defined by photolithography. This PDMS stamp was assembled with glass cover slip by cleaning the glass slip with piranha solution, and treating the stamp with oxygen plasma. The oxygen plasma provides hydrophilic surface to the PDMS stamp that helps to bond with the glass substrate strongly. The soft PDMS also allows us to create inlet and outlet by using the syringe needle. The nanowires are mechanically transferred on the cover slip so that nanowires can be imaged to monitor the sequential surface reactions using solution-phase reagents. Figure 2.6 shows the schematic of microfluidic device and a real picture of the device.

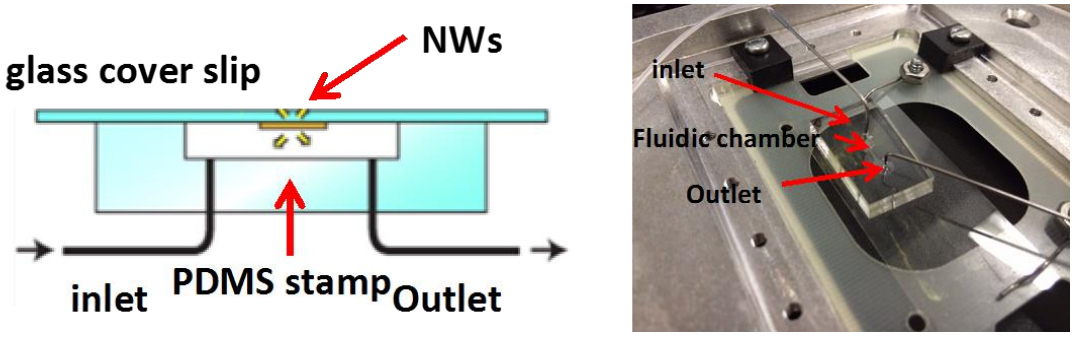

Figure 2.6 Schematics and image of microfluidic device showing inlet and outlet

2.3.1 His-tagged protein as a ligand

Grx4 protein (~13.7kDa), which is tagged with poly histidine group and has 3 cysteine and 7 lysine residue was used as a ligand for this experiment. Histidine tagged protein was chosen to measure the adsorption and desorption rate because it has already been shown that histidine tagged protein can bind to metal sulfide surface through metal affinity interactions between imidazole nitrogen and surface cadmium atoms[24]. Similar procedure was used to label the protein with rhodamine dye as in the case of terpolymer.

After transferring VLS grown nanowires in to the cover slip, the microfluidic device was fabricated. PH 8.4 $NaHCO_3$ aqueous solution was used as a solvent for protein as well as dye free solution to wash off the ligands. For first 5 minutes, the dye free bicarbonate solution was flown in order to remove any free wires, or dust. After 5 minutes, 6 µM solution of dye labeled protein was flown at 0.375 mL/min until all the available sites were filled with protein, which was evident from the fluorescence picture being captured by camera every 5 seconds. The concentration of dye labeled polymer was calculated using dye concentration as given by UV-Vis spectrum. The excitation

wavelength was 510 nm, and emission filter was long pass 590 nm so that fluorescence from nanowires can be cut off and only dye emission can be collected. All the images were analyzed by using mat lab software. While analyzing the image, a particular section of nanowire is selected using dark field image, and corresponding fluorescence images are analyzed to get the intensity value of red channel with respect to time. The local and global background of the images are subtracted in order to get net fluorescence intensity coming from the bound ligands. Figure 2.7 shows the region of interest of the nanowires in red channel of the fluorescence image(A), fluorescence intensity with respect to time during adsorption of ligand on nanowires(B), fluorescence intensity during washing of the ligand(C), and natural log of the fluorescence intensity during adsorption with respect to time(D).

When ligands are continuously supplied, the intensity of signal rises, until all the available sites are saturated. During the adsorption of ligands on the nanowire surface, at particular time, the fluorescence signal intensity can be given as:

$$[BL]_t = [BL]_e (1 - e^{-k_{app}*t})$$

Where, $k_{app} = k_{on}[L] + k_{off}$

From the curve in Figure 2.7(B), k_{app} can be calculated to be $5.85X10^{-2}$ s^{-1}. At two different protein concentration, k_{on} and k_{off} can be calculated. Also from first order kinetics, during washing off the ligands,

$$\ln[[BL]_t - [BL]_\alpha] = -k_{off}t + \ln[BL]_e$$

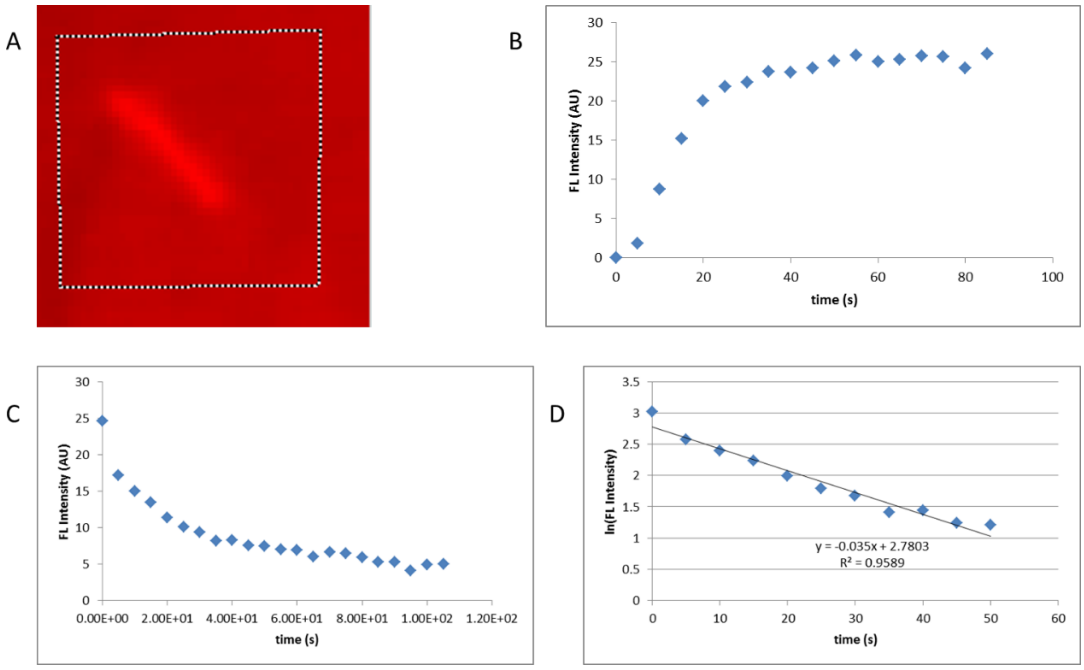

Figure 2.7 Kinetic data of protein binding on nanowire surface. A: region of interest in the fluorescence image. B: fluorescence intensity with respect to time during adsorption of ligand on nanowires. C: fluorescence intensity during washing of the ligand. D: natural log of the fluorescence intensity during adsorption with respect to time.

Where, $[BL]_{\alpha}$ is the minimum intensity after washing off the ligands. This equation is in the form of y=mx+c, and the slope of line gives $-k_{off} = 0.035\ s^{-1}$. Since, we have k_{app}, and k_{off}, k_{on} can be calculated to be $3.84X10^{3}M^{-1}s^{-1}$. Using k_{on} and k_{off}, the binding constant can be calculated to be $1.97X10^{5}\ M^{-1}$.

By using different concentrations of ligands, the obtained binding constant can be confirmed. Even though we were successfully able to calculate the binding constant of protein on nanowire surfaces, various challenges were seen during the experiment. The most important problem was unspecific binding of polymer on the glass surfaces. This

actually increased the background of the signal, and decreased the signal coming from bound dye labeled polymer. In order to solve this problem, we chose polymeric ligand with imidazole group which has been confirmed by ourselves to bind on the nanowire surface. The other problem while performing this study was nanowires are lying flat on the surface of cover slip. Therefore, the ligand solution was not accessible throughout the surfaces of nanowires. So, a better set up with the trenches on coverslip will help to get better signal from nanowires, as all the surfaces of nanowires will be accessed with the ligand solution.

2.3.2 Terpolymer as a ligand

In order to solve the problem of nonspecific binding, terpolymer was chosen as a ligand. The terpolymer has three different functional groups: PEG group to provide water solubility to the polymer, imidazole group to attach to the nanowire surfaces, and primary amine group to attach fluorescence dye. The conjugation of polymer dye is already explained above, and the concentration of dye labeled polymer was used by looking at dye concentration as given by UV-Vis Spectrum. Using the published extinction coefficient of rhodamine dye, and the absorbance value of purified dye labeled polymer, 0.25 dye per polymer was calculated.

The similar approach was used to study binding of terpolymer on nanowire surface as protein. The concentration of terpolymer was 200 nM, and the flow rate was set to 0.4mL/min. The buffer solution was first flown, followed by the ligand solution. The attached ligands were washed off by aqueous $NaHCO_3$ solution. Figure 2.8 shows

curve of intensity of fluorescence over time (A), and natural log of intensity during desorption phase (B).

During the adsorption of ligands on the nanowire surface, at particular time, the fluorescence signal intensity can be given as:

$$[BL]_t = [BL]_e (1 - e^{-k_{app}*t})$$

Where, $k_{app} = k_{on}[L] + k_{off}$

From the curve in Figure 2.8(A), k_{app} can be calculated to be $3.63X10^{-4}$ s^{-1}. At two different concentration of ligand, k_{on} and k_{off} can be calculated. During the desorption phase,

$$\ln[[BL]_t - [BL]_\alpha] = -k_{off}t + \ln[BL]_e$$

k_{off} can be calculated as a slope of the line in figure 2.8(B), which is 0.008 s^{-1}. For 200 nM polymer ligand, k_{on} can be calculated as $1.4170X10^4$ $M^{-1}s^{-1}$. From k_{on} and k_{off} binding constant can be calculated to be $3.89x\ 10^7\ M^{-1}$.

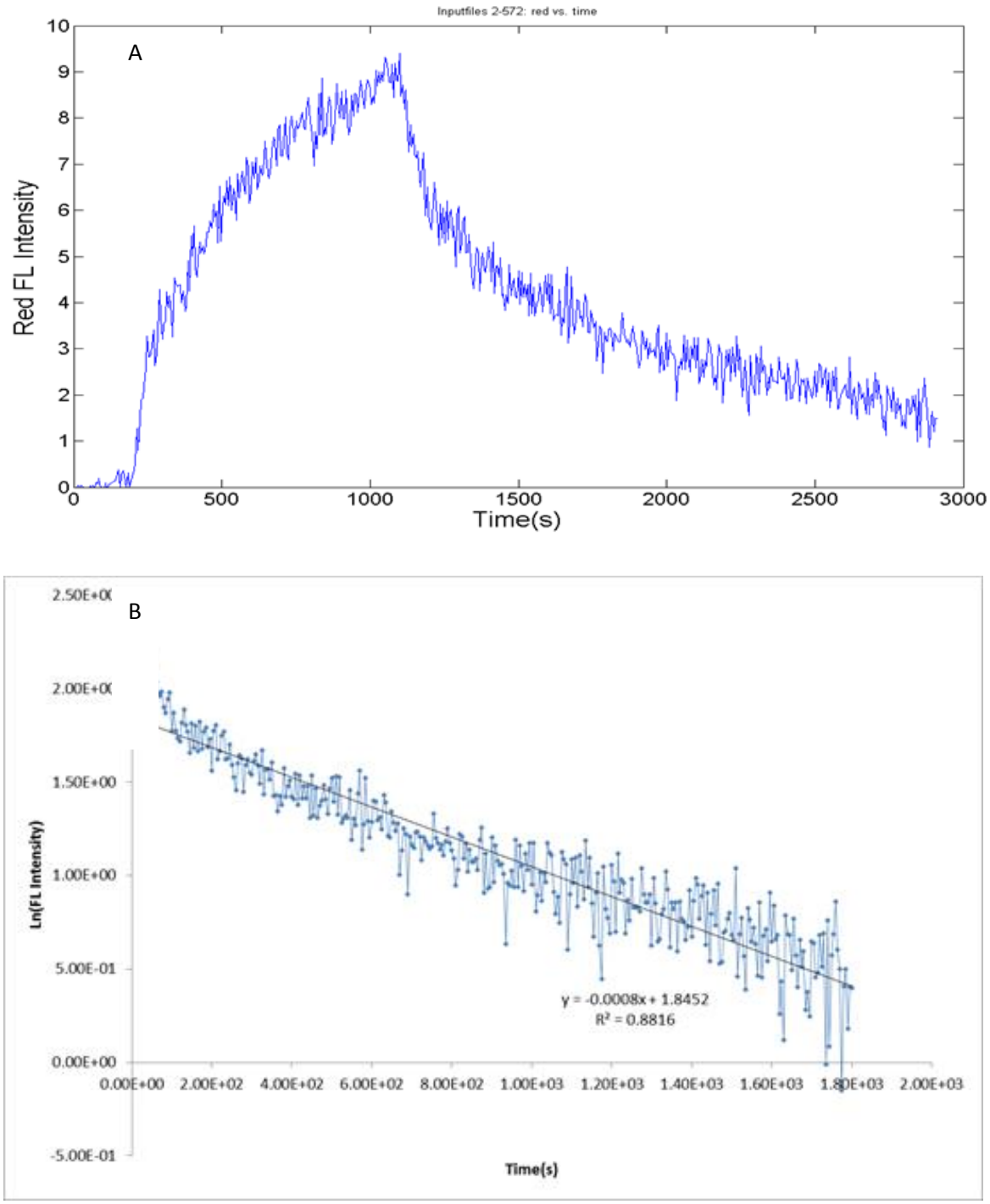

Figure 2.8 Intensity of fluorescence during adsorption and desorption phase with respect to time (A), and natural log of fluorescence with respect to time during desorption phase (B).

2.4 CONCLUSION

This study shows that methacrylate-based polymeric imidazole ligands can coordinate with vapor deposited CdS NW surfaces. This has been demonstrated by binding fluorescence dye on the ligand and attach the ligands on the NWS surface. Fluorescence microscopy was used to demonstrate the ligand binding on nanowire surfaces. This approach has been extended to study the ligand binding kinetics on nanowire surfaces. Adsorption and desorption constant of ligand binding on nanowire surfaces has been calculated. In order to get better results nonspecific binding of ligands on nanowires and background should be minimized. This study opens the door to various other ligands that can be bound to nanowire surfaces which can alter optoelectronic properties of the nanowires. These studies can also be extended on various other compound semiconductors with different functional needs.

References

(1) Li, Z.; Ma, X.; Sun, Q.; Wang, Z.; Liu, J.; Zhu, Z.; Qiao, S. Z.; Smith, S. C.; Lu, G. (Max); Mews, A. *Eur. J. Inorg. Chem.* **2010**, *2010* (27), 4325–4331.

(2) Sun, M. H.; Joyce, H. J.; Gao, Q.; Tan, H. H.; Jagadish, C.; Ning, C. Z. *Nano Lett.* **2012**, *12* (7), 3378–3384.

(3) Wang, P.; Zhang, J.; He, H.; Xu, X.; Jin, Y. *Nanoscale* **2015**, *7* (13), 5767–5775.

(4) Xie, Z.; Markus, T. Z.; Gotesman, G.; Deutsch, Z.; Oron, D.; Naaman, R. *ACS Nano* **2011**, *5* (2), 863–869.

(5) Xiao, M. X.; Zhao, M.; Jiang, Q. *Chem. Phys. Lett.* **2011**, *512* (4–6), 251–254.

(6) Pemasiri, K.; Montazeri, M.; Gass, R.; Smith, L. M.; Jackson, H. E.; Yarrison-Rice, J.; Paiman, S.; Gao, Q.; Tan, H. H.; Jagadish, C.; Zhang, X.; Zou, J. *Nano Lett.* **2009**, *9* (2), 648–654.

(7) Lauhon, L. J.; Gudiksen, M. S.; Lieber, C. M. *Philos. Trans. R. Soc. Lond. Math. Phys. Eng. Sci.* **2004**, *362* (1819), 1247–1260.

(8) Tang, J.; Huo, Z.; Brittman, S.; Gao, H.; Yang, P. *Nat. Nanotechnol.* **2011**, *6* (9), 568–572.

(9) Tian, B.; Zheng, X.; Kempa, T. J.; Fang, Y.; Yu, N.; Yu, G.; Huang, J.; Lieber, C. M. *Nature* **2007**, *449* (7164), 885–889.

(10) Shen, Y.; Tan, R.; Gee, M. Y.; Greytak, A. B. *ACS Nano* **2015**, *9* (3), 3345–3359.

(11) Anderson, N. C.; Owen, J. S. *Chem. Mater.* **2013**, *25* (1), 69–76.

(12) Yun, H. J.; Paik, T.; Edley, M. E.; Baxter, J. B.; Murray, C. B. *ACS Appl. Mater. Interfaces* **2014**, *6* (5), 3721–3728.

(13) Knowles, K. E.; Tice, D. B.; McArthur, E. A.; Solomon, G. C.; Weiss, E. A. *J. Am. Chem. Soc.* **2010**, *132* (3), 1041–1050.

(14) Owen, J. S.; Park, J.; Trudeau, P.-E.; Alivisatos, A. P. *J. Am. Chem. Soc.* **2008**, *130* (37), 12279–12281.

(15) Anderson, N. C.; Hendricks, M. P.; Choi, J. J.; Owen, J. S. *J. Am. Chem. Soc.* **2013**, *135* (49), 18536–18548.

(16) Schreuder, M. A.; McBride, J. R.; Dukes, A. D.; Sammons, J. A.; Rosenthal, S. J. *J. Phys. Chem. C* **2009**, *113* (19), 8169–8176.

(17) Collins, G.; Fleming, P.; Barth, S.; O'Dwyer, C.; Boland, J. J.; Morris, M. A.; Holmes, J. D. *Chem. Mater.* **2010**, *22* (23), 6370–6377.

(18) Gleason-Rohrer, D. C.; Brunschwig, B. S.; Lewis, N. S. *J. Phys. Chem. C* **2013**, *117* (35), 18031–18042.

(19) Hang, Q.; Wang, F.; Carpenter, P. D.; Zemlyanov, D.; Zakharov, D.; Stach, E. A.; Buhro, W. E.; Janes, D. B. *Nano Lett.* **2008**, *8* (1), 49–55.

(20) Kim, D. K.; Fafarman, A. T.; Diroll, B. T.; Chan, S. H.; Gordon, T. R.; Murray, C. B.; Kagan, C. R. *ACS Nano* **2013**, *7* (10), 8760–8770.

(21) Li, X.; Nichols, V. M.; Zhou, D.; Lim, C.; Pau, G. S. H.; Bardeen, C. J.; Tang, M. L. *Nano Lett.* **2014**, *14* (6), 3382–3387.

(22) Greytak, A. B.; Allen, P. M.; Liu, W.; Zhao, J.; Young, E. R.; Popović, Z.; Walker, B. J.; Nocera, D. G.; Bawendi, M. G. *Chem. Sci.* **2012**, *3* (6), 2028.

(23) Liu, W.; Greytak, A. B.; Lee, J.; Wong, C. R.; Park, J.; Marshall, L. F.; Jiang, W.; Curtin, P. N.; Ting, A. Y.; Nocera, D. G.; Fukumura, D.; Jain, R. K.; Bawendi, M. G. *J. Am. Chem. Soc.* **2010**, *132* (2), 472–483.

(24) Sapsford, K. E.; Pons, T.; Medintz, I. L.; Higashiya, S.; Brunel, F. M.; Dawson, P. E.; Mattoussi, H. *J. Phys. Chem. C* **2007**, *111* (31), 11528–11538.

CHAPTER 3

CONSEQUENCES OF SURFACE TREATMENT ON NANOWIRE ELECTRONIC AND OPTICAL PROPERTIES

3.1 INTRODUCTION

Semiconductor nanowires have been widely studied due to their unique properties such as width comparable to critical length-scales, high aspect ratio, and high carrier mobility. These unique properties make them a suitable candidate for various optical and electronic devices like photovoltaics, photodetectors, and field effect transistors. The nanowire surface plays an important role in the performance of these devices, because of their high surface to volume ratio. The increased surface area of nanowires may provide better charge separation by providing shorter distance for carriers to move before collection. However, the presence of surface states may lead to trap states within the band gap, trapping the photogenerated electrons and holes and decreasing the efficiency of charge separation. These surface states may arise from unsaturated atoms on the surface of the crystal. One way to saturate these unsaturated atoms is by forming bonds to ligands on the surface.

Various ligands have been used to modify the surfaces of colloidal nanocrystals and bulk materials. These ligands have been shown to tune various electronic properties. Our goal is to use the surface chemistry developed for colloidal nanocrystal

and bulk materials and use them on semiconductor nanowires. In this work, metal chalcogenide II-VI nanowires, grown via the high-temperature vapor liquid solid process, which yields highly crystalline nearly defect free wires, are treated following growth with solution phase and vapor phase reagents to control the chemical state of their surfaces.

We are particularly interested in tuning three electronic properties of nanowires by binding ligands on the nanowire surfaces: non radiative recombination, surface trapping and surface potential. Non radiative recombination, particularly surface recombination can be decreased or increased by binding ligands on the nanowire surfaces. This increase or decrease of non-radiative recombination can be probed by comparing the photoluminescence intensity of the band edge emission or by looking at the photocurrent at constant bias. Similarly, surface trapping can be studied by the persistent photocurrent measurement and by calculating subthreshold slope. Subthreshold slope can be calculated by studying gate dependent current. Surface potential built by the localized charge can be studied by looking at threshold voltage. Photocurrent, persistent photocurrent, subthreshold slope, and threshold voltage can be calculated by fabricating nanowire field-effect transistors.

Even though a lot of work has been done to modify the surfaces of nanocrystals, limited work has been done on the nanowire surface due to various challenges. The biggest challenge is that nanowires are not soluble in any solvent because of their size. This limits many techniques such as NMR, UV-Vis, mass spectrometry, that are used to detect ligand binding on the colloidal semiconductor surfaces. However, we can use some other techniques such as XPS, fluorescently labelled ligands, IR, and Raman to

detect the surface chemical changes on the nanowires. As a proxy, we can detect those surface chemical changes by detecting changes in electronic properties concurrent with chemical treatment. Another challenge with nanowires is to synthesize nanowire with consistent properties. We chose high temperature VLS growth method to grow low defect nanowires. These nanowires need to have a recognizable surface condition, similar composition, and similar diameter in order to obtain repeatable and accurate results. This problem can be solved by simultaneously producing two samples, a control sample and treated sample, or performing a before and after measurement using a gas phase treatment. We need many devices to differentiate the electronic properties of control and treated sample. Therefore, to obtain many devices, we chose a simple, homemade mechanical transfer system that can transfer large amount of nanowires and align them in the same direction. Our VLS grown nanowires have a native surface, therefore, it is also necessary to manage the device atmosphere, as CdS nanowires can form a thin layer of native oxide on the surface that can hinder the access of ligands or can deplete the electron decreasing the conductivity of a nanowire.[1]

To study the consequences of ligand binding on nanowire optical and electronic properties, photoluminescence and transport measurements are performed. Photoluminescence is a simple nondestructive measurement which can reveal the composition of the material, its band gap, and the presence of surface states. This measurement will show if ligands can increase quantum yield for radiative recombination and if surface traps are removed or created after surface treatment. Similarly, transport measurement will give the electronic properties of nanowires such as surface trapping, and surface potentials.

3.2 PHOTOLUMINESCENCE MEASUREMENT:

Photoluminescence is a common way to study the opto-electronic structure of semiconductors. It is a contactless and nondestructive technique. When light with appropriate energy is absorbed by a semiconductor, an electron and hole pair is generated. The electron excites to the conduction band, and holes stay in the valence band. If the charges are not separated, the electrons and holes recombine. This recombination can be radiative, by emitting light equal to the band gap energy, or non-radiative. Trap states and several surface states present in the semiconductor contribute to non-radiative recombination. Photoluminescence helps to determine the band gap of semiconductor by monitoring the spectral distribution of photoluminescence, which may reveal the elemental composition of semiconductor. It also provides the information about the presence of impurities and recombination mechanism.

Our lab is equipped with a photoluminescence measurement set up including different excitation wavelength and ocean optics USB 4000 detector. We have a lamp as an excitation source equipped with 365 nm short pass filter connected to an optical microscope. At around 365 nm, CdS has the largest absorption. This excitation source is also good for taking fluorescence images of CdS nanowires as it is a part of microscope set up. In order to take the fluorescence spectra from the microscope set up, we have fiber-optic pick up of the emission light that is detected by an ocean optics USB 400 detector. We also use a 440 nm diode laser as an excitement source to study the photoluminescence measurement, as it is higher in energy than the band gap of CdS nanowire that corresponds to ~505 nm. We also have the capability to measure solid state fluorescence both inside and outside inert atmosphere if needed. In order to study the

consequences of ligand binding on the nanowire surface we performed photoluminescence measurements before and after ligand binding to observe the differences in intensity of band edge emission, band edge shift, and appearance and disappearance of sub band gap emission peaks. This measurement will show the effects of ligand binding on nanowire surfaces, which can be further confirmed by performing the transport measurement of the nanowire devices.

We chose CdS nanowires to perform ligand binding experiment because surface chemistry of CdS nanocrystal has been extensively investigated. Also, CdS is a highly abundant direct band gap semiconductor which makes it a potential candidate for light harvesting and other electronic devices. We chose VLS grown CdS nanowires because these nanowires have very low defect and higher photoluminescence. Our nanowires are roughly 40-200 nm in diameter. This part of the chapter will explore various ligands that have been previously used in colloidal nanocrystals, bulk, or nanowires, and will show the consequences of their attachment in the CdS nanowire surface. We chose a phosphonic acid, a thiol, aniline and chloride as ligands for CdS nanowires because they have been used in case of colloidal nanocrystal or bulk, and they have been shown to change the non-radiative recombination as evident by photoluminescence measurement. We want to see if these changes observed in the colloidal system and bulk can be seen in case of CdS nanowires with native surface.

3.2.1 Treatment with octadecylphosphonic acid

Phosphonic acid has been commonly used as a ligand on colloidal nanocrystals.[2,3] Phosphonic acids have already been shown to affect the growth kinetics and shape of the

nanocrystals.[4,5] It has also been shown that depending upon the type of phosphonic acid, emission of CdSe nanocrystal can be pinned at different wavelength.[6] The extent of pinning depends upon the alkyl length and the electronegativity of phosphonic acid ligands.

We chose octadecylphosphonic acid as a ligand to attach to CdS native surface because phosphonic acid can attack CdO, and may be able to form a strong bond to surface and remove any native oxide. Octadecylphosphonate can also strongly binds to the cadmium surface making cadmium octadecylphosphonate. Two growth substrates of the same batch were taken, and photoluminescence images and spectra of nanowires on both substrates were recorded. One substrate was dipped in a solution containing octadecylphosphonic acid (ODPA) in octadecene, and the other control substrate was dipped in octadecene. Both substrates were dipped in solution for 2 hours at around 100ºC in nitrogen atmosphere, and were rinsed with fresh solution of octadecene and DI water and dried by nitrogen gas. After treatment fluorescence images and spectra were taken. The fluorescence image and spectra of the control chip are close to identical before and after treatment. However, as shown in Figure 3.1, the photoluminescence image after modification is brighter and the intensity of bandgap emission in the recorded spectrum increases as well. The emission peak is around 505 nm that corresponds to band edge emission. This result shows radiative recombination increases with the introduction of octadecylphosphonic acid to native CdS nanowire. XPS can be done on the treated nanowires in order to confirm the association of ODPA in the CdS nanowire surface. Similarly, transport measurement can be done to see if the ligand has any impact on surface trapping and surface potential.

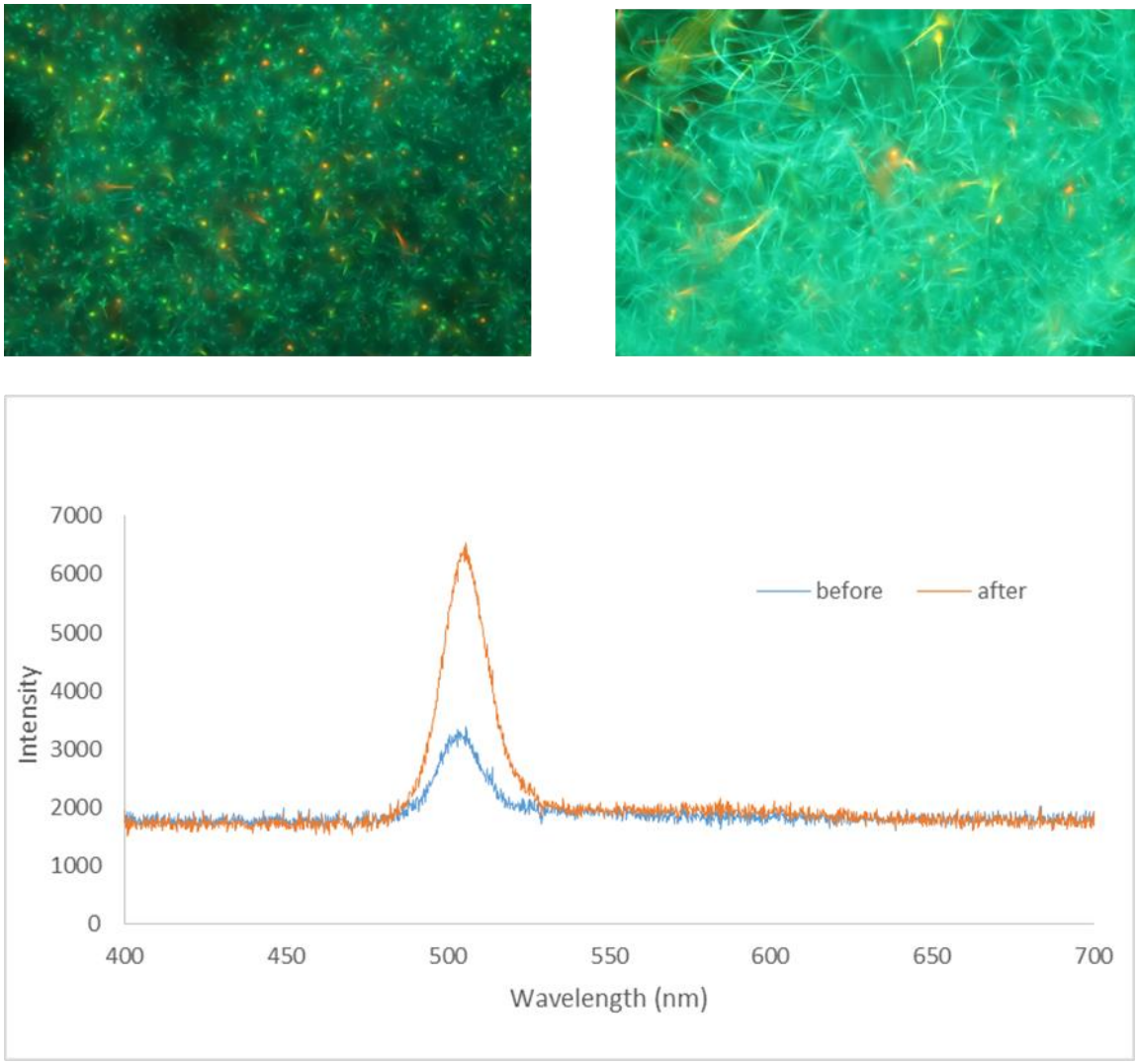

Figure 3.1 FL image of CdS nanowires before and after modification with octadecylphosphonic acid (Top), and PL spectra of CdS nanowires before (blue), and after (orange) surface medication using octadecylphosphonic acid (Bottom). The spectra shows increase in band edge emission after treating the surface. The excitation wavelength is 365 nm.

3.2.2 Treatment with cysteine

Cysteine is commonly used as a ligand in colloidal nanocrystals.[7,8] It has been shown that the introduction of L-cysteine in CdSe/ZnSe quantum dots in aqueous solvent enhances the photoluminescence significantly.[9] The adsorption of the cysteine molecule to the quantum dots surface occurs through amine functional group and deprotonated thiol.[9] Cysteine ligand has been used in nanocrystals to get biocompatible nanocrystals.[10]

Cysteine binds with CdS nanowires with amine group or by deprotonated thiol group by forming a dative covalent bond. In order to see if the thiol increases or decreases non-radiative recombination, cysteine was used to treat CdS nanowires. Two nanowire growth substrates with identical growth parameter were taken and their fluorescence image and photoluminescence spectra were recorded. One substrate was dipped in a 50 mM solution of cysteine in water for 2 hours. Another substrate, as a control, was dipped in water for 2 hours. After 2 hours, both substrates were rinsed, dried and measured. The fluorescence image and photoluminescence spectra of control substrate were almost identical. However, as shown in figure 3.2, the fluorescence of cysteine treated nanowires decreased significantly at the band gap indicating an increase in non-radiative recombination. The peak at around 505 nm indicates band gap emission. The successful binding of cysteine on nanowire can be confirmed by using other techniques like IR and Raman. Their consequences in electronic properties can also be confirmed by looking at photocurrent and persistent photocurrent.

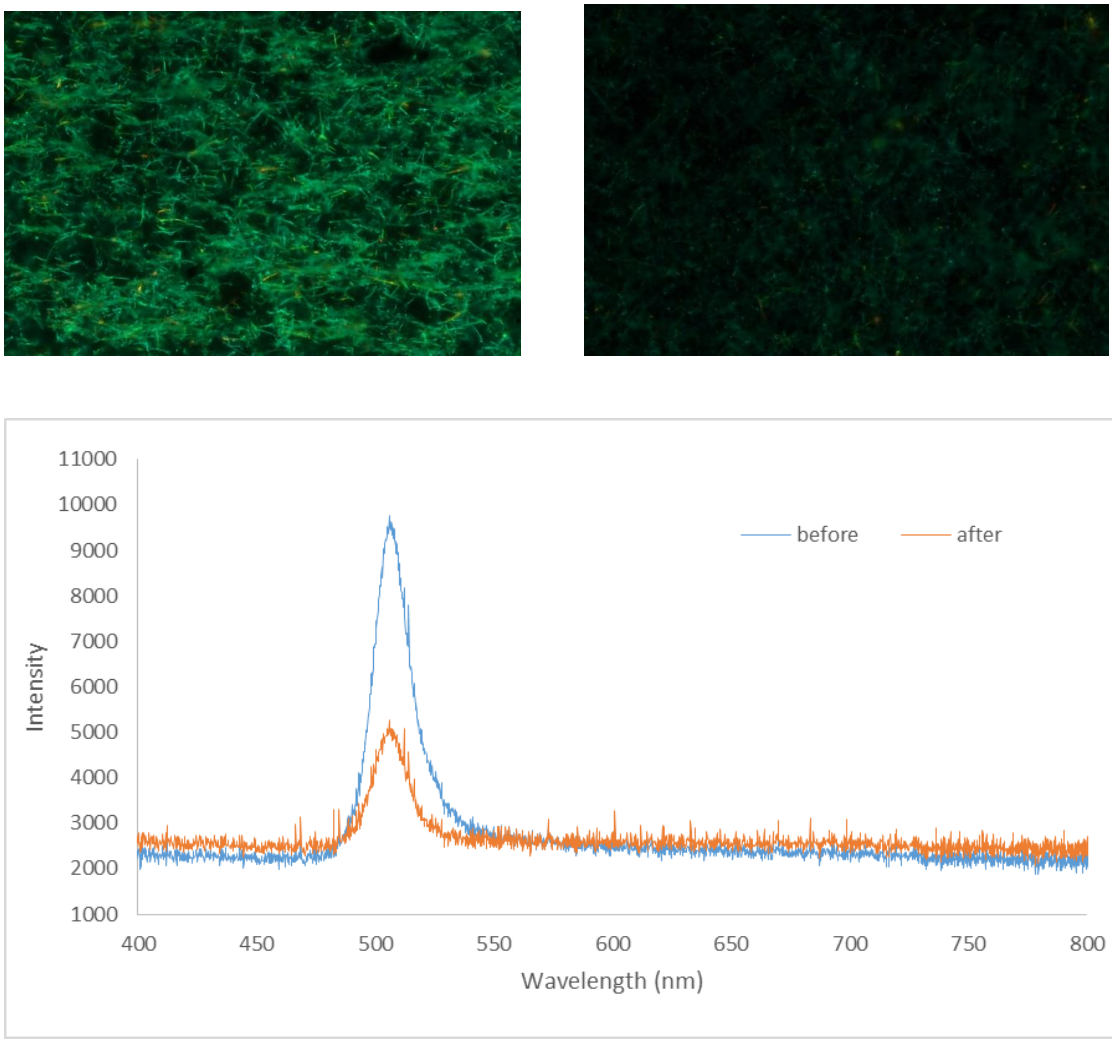

Figure 3.2 FL images of CdS nanowires before and after treatment with L-cysteine (Top), and PL spectra of CdS nanowires before modification (blue), and after modification with L-cysteine (orange). Excitation wavelength is 365 nm.

3.2.3 Treatment with HCl

Nanocrystal electronic devices are normally fabricated using nanocrystal films. For this application, long organic ligands are replaced by short chloride ligands. The Murray group has shown that replacing the bulky organic layers with a sulfide ligand increases the charge transfer efficiency in CdSe QD sensitized solar cells by removing

the insulating organic barrier.[11] Similarly it has also been shown that HCl treatment of Ge nanowires results in chloride terminated surfaces.[12,13]

Depending the concentration of HCl, the surface of CdS nanowires can be terminated with anionic chloride ligand, or etched. SEM can reveal if the nanowire surfaces are etched or not by looking at the roughness of the surface. We can use XPS to reveal if the surface is terminated with chloride ion or not. The etching is possible because of the solubility of $CdCl_2$ in water. In order to study the consequences of surface treatment of HCl on CdS nanowires, fluorescence images and photoluminescence measurement of as grown nanowires were taken using 365 nm excitation light. The substrate containing nanowires was dipped in 0.1M HCl for 5 seconds, rinsed with water, blown dry with nitrogen gas, and measured. Figure 3.3 shows the fluorescence image of nanowires before and after treatment with HCl. The band gap emission peak at around 505 nm decreases significantly after treating the nanowire surface with HCl solution. The red fluorescence in the image and sub band gap emission between 600 to 750 nm represents sub band gap emission. The sub band gap emission represents the introduction of trap in the nanowire surface after treating the surface with HCl solution.

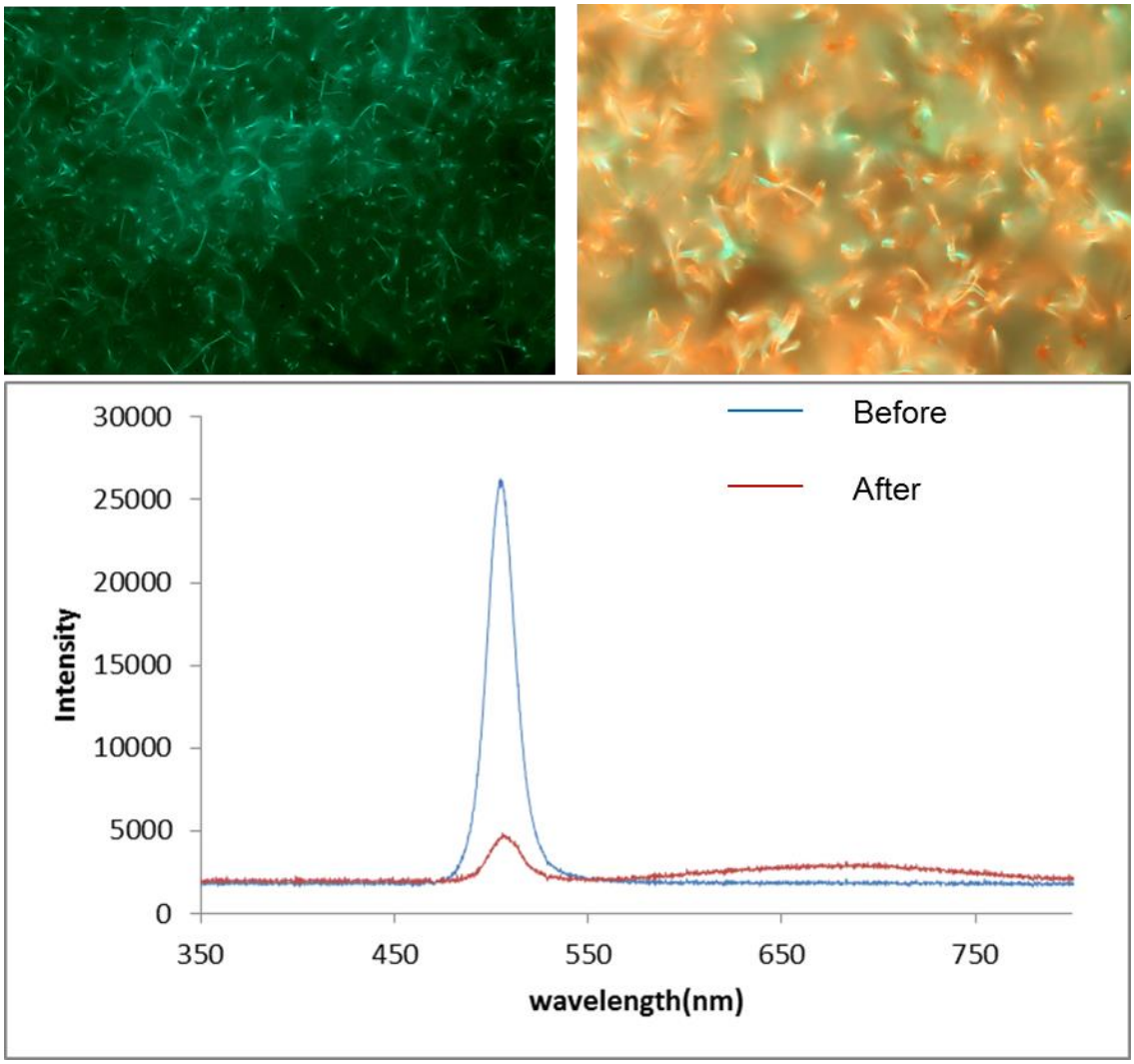

Figure 3.3 FL images of CdS nanowire before and after treating with HCl (Top), and PL spectra of as grown (blue), and after treated (red) nanowires (Bottom). Treatment of HCl on nanowire surfaces introduces sub band gap emission. The excitation wavelength is 365 nm.

3.2.4 Treatment with aniline

Aniline and various substituted anilines have already been used as ligands on bulk crystals and nanocrystals.[14,15] It has been shown in the case of CdS and CdSe bulk crystals that different substitutes of aniline affect the photoluminescence by effecting the

charge transport from the surface states to the bulk crystals.[15] The unsaturated cadmium ions in these crystals act as trapping sites, which creates a depletion region by the localized charge electrostatics. Depending on the substitutes of aniline, this depletion region is contracted or expanded. In case of colloidal CdSe nanocrystals, substituted anilines decrease the photoluminescence when they replace the original ligands present in nanocrystals.[14] These ligands passivate cadmium surface site, and quench the photoluminescence through hole transfer.

We chose anilines to treat the surface of CdS nanowires as they have been shown to change the non-radiative recombination in bulk and colloidal nanocrystals. They can bind to the nanowire surface through amine functional group. Anilines are volatile, neutral molecules which potentially permits binding and release experiments under gas flow. We built up an in situ measurement set up where we can monitor the changes in photoluminescence over time as aniline is continuously supplied to the CdS nanowires. The schematic of this is shown in figure 3.4. The nanowires on the growth substrate are attached inside a polydimethyl siloxane (PDMS) stamp. This PDMS stamp is attached with a glass cover slip to assemble the device such as nanowires can be observed through the cover slip, and photoluminescence measurement can be done through the top of coverslip. The fluorescence probe is located above the nanowires that are excited with a 440 nm laser. Nitrogen is bubbled in to the aniline solution, and the nitrogen/aniline gas is fed to the PDMS chamber through an inlet. The outlet gas is fed in to a diluted HCl solution to scrub the gas. The aniline/nitrogen gas can be replaced with pure nitrogen to study the desorption of aniline from nanowire surface. This set up has the possibility of

studying kinetics of aniline adsorption and desorption and can be extended to various substituted anilines.

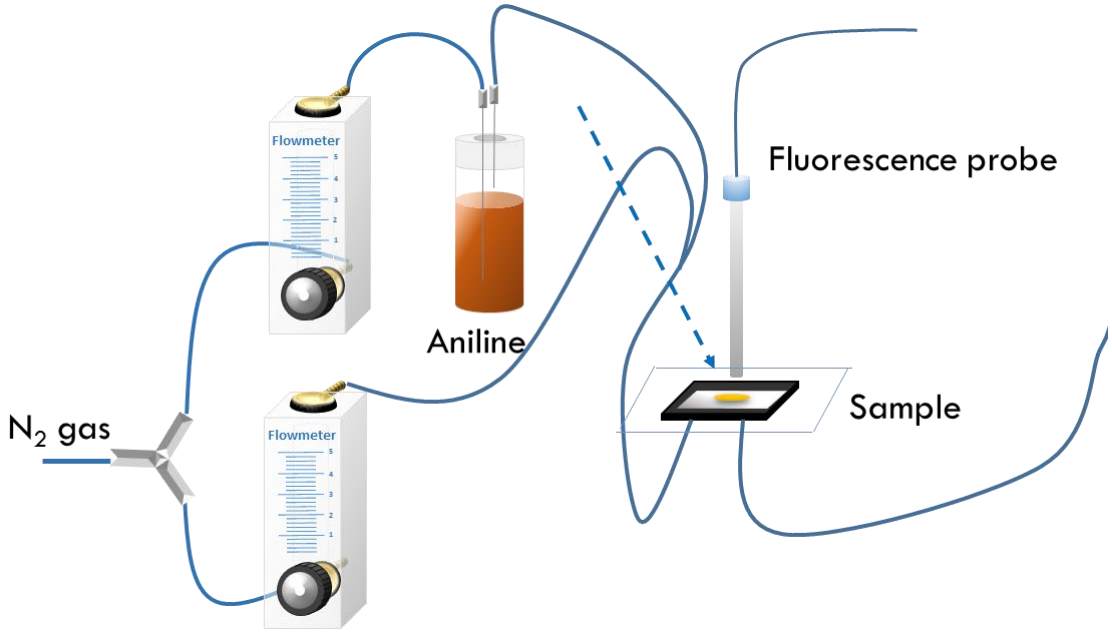

Figure 3.4 Schematic of set up for studying the change in fluorescence overtime when aniline vapor is flown through CdS nanowires. The aniline gas is produced by bubbling the nitrogen in aniline solution.

Figure 3.5 shows the photoluminescence spectra of CdS nanowires before and after treating with aniline in two different experiments. In the first experiment, the photoluminescence measurement was done with as grown CdS nanowires that were treated with aniline vapor for 25 minutes. The top of Figure 3.5 shows the photoluminescence spectra of as grown and aniline treated nanowire. The PL of CdS nanowire treated with aniline almost doubles indicating the similar result observed in bulk CdS/CdSe. The bottom of the figure shows the maximum intensity of fluorescence

taken at 504 nm with respect to time. The nanowires are treated continuously with aniline vapor, and photoluminescence spectrum is taken every minute. Before flowing aniline vapor, nitrogen is passed through the wires. With the introduction of nitrogen, photoluminescence increases slightly, and then stay flat after few minutes. The increase in fluorescence is because of the depletion of oxygen in the system or adsorbed oxygen in the nanowire surfaces. After that, aniline/nitrogen vapor is passed through the device, and photoluminescence spectra are recorded overtime. It is clearly visible from graph that photoluminescence intensity of CdS nanowire increases overtime when treated with nanowire until all the available binding sites are saturated. This result indicates that the aniline is saturating unbound cadmium sites, which enhances the photoluminescence by removing the surface state. The same experiment can be performed to see the desorption of aniline from nanowire surface overtime by looking at the photoluminescence spectra overtime.The transport measurement will reveal more about the surface trapping in the surface and surface potential created by localized charge electrostatics.

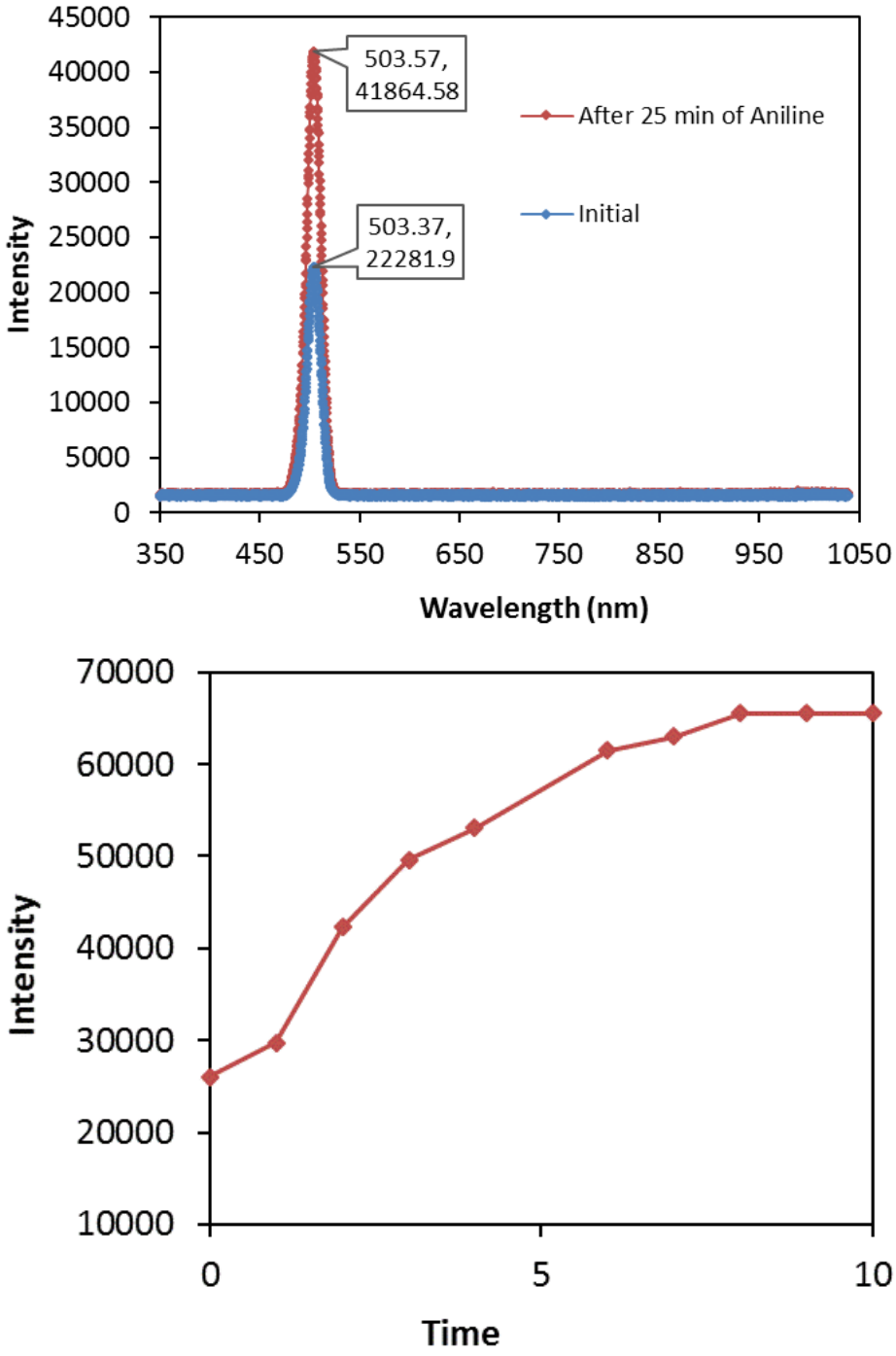

Figure 3.5 Comparison of photoluminescence before and after 25 minutes of treatment of aniline in CdS nanowires (Top), and intensity of maximum fluorescence at 504 nm with respect to the time when aniline is introduced in CdS nanowires (Bottom).

3.3 TRANSPORT MEASUREMENT

Transport measurement can be performed in order to study the electronic properties of semiconductor nanowires. Unintentionally doped CdS nanowires are intrinsic semiconductors with very low carrier concentration. Transport measurements of nanowires can be done using nanowire transistor devices. The dark current-voltage measurement gives an idea about the carrier concentration of the semiconductor and the contact resistance between the metal and nanowires interface. The conductivity of the nanowires and threshold voltage of the device can be calculated. Similarly, measuring the photocurrent can reveal the photo conversion efficiency, which can be compared before and after ligand binding on nanowire surfaces. The photocurrent measurement using an optical chopper can be performed to see the on/off ratio of the device as well as any persistent photocurrent. These measurements can provide information about non radiative recombination, surface trapping and surface potential of the nanowires.

3.3.1 Nanowire device fabrication

CdS nanowires are grown on a silicon substrate with a native oxide layer using the VLS mechanism. CdS powder is used as a precursor, and argon gas is used as a carrier gas. The detail of the growth procedure is explained in Chapter 1 of this thesis. After growth, nanowires are transferred from the growth substrate to a silicon substrate with a 400 nm oxide layer deposited. In order to get many functional devices we need to transfer high density of nanowires and align them in proper direction. In order to achieve this, we chose simple mechanical transfer method. In this process, first, the receiver substrate is rinsed with acetone and water and dried with nitrogen gas. The receiver substrate, with oxide layer facing up is temporarily attached to the cover slip that is lying

flat on the surface. The growth substrate is also attached with another coverslip with nanowires facing top. The coverslip with growth substrate is brought in contact with receiver substrate, and pushed gently in one direction to mechanically transfer the nanowires. The receiver substrate is detached from the coverslip, rinsed with DI water and dried with nitrogen. The Figure 3.6 shows the SEM images of nanowires in the growth substrate and mechanically transferred nanowires in the receiver substrate. The nanowires after transfer align horizontally on the substrate.

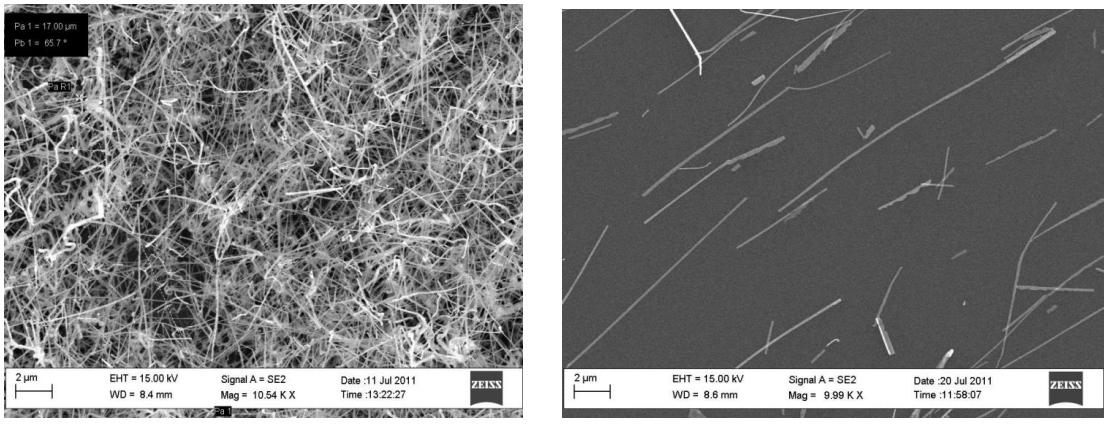

Figure 3.6 SEM image of CdS nanowires in the growth substrate (left), and mechanically transferred nanowires after growth (right)

The next step in device fabrication is photolithography. Before depositing the photoresist, the substrate is dried at 180 ^{o}C in air for 5-10 minutes. After drying, liftoff resist LOR3A and photoresist AZ5214 are deposited one after another. The approximate thickness of LOR3A is 0.4 µm, and AZ5214 is 1.25 µm. After a short bake, a mask aligner is used to expose the substrate. The exposure is done around 8-10 seconds with UV-lamp. After the exposure, the substrates are developed using a 1:4 solution of AZ400 developer solution and DI water. The development time varies from 25-60 seconds. The

exact development time can be confirmed by periodically looking at the substrate until the patterns are whitish and not greenish or reddish. The patterns can be confirmed using a microscope with appropriate filter, and longer development can be done if the substrate is found poorly developed.

Metal contacts are deposited using electron beam physical vapor deposition. For the CdS nanowires grown in our lab, 30 nm of titanium followed by 70 nm of gold are deposited as electrodes to get ohmic contacts. Even though when CdS surface comes in contact with Ti surface, it should form the ohmic contact, it is not the case every time. I-V curve of our device does not show ohmic contact. There are various surface states present in the semiconductor which trap the carriers and build up the electrostatic charge in the surface. This surface potential bends the energy bands of the semiconductor resulting in non-ohmic contact. People have used argon ion bombarding on the contact region of CdS nanowires to get ohmic contact with Ti by introducing donor type impurities.[16] Same results have been obtained in our lab. Figure 3.7 shows the band diagram of CdS and Ti/Au electrodes showing semiconductor-metal ohmic contacts (left), and various steps involved in device fabrication (right). Metal deposition is followed by lift off. For the liftoff process, the substrates are dipped in Remover PG liftoff solution for an hour and are sonicated gently for a minute in fresh lift off solution. The substrate is rinsed with clean lift off solution and water and blown dry with nitrogen gas.

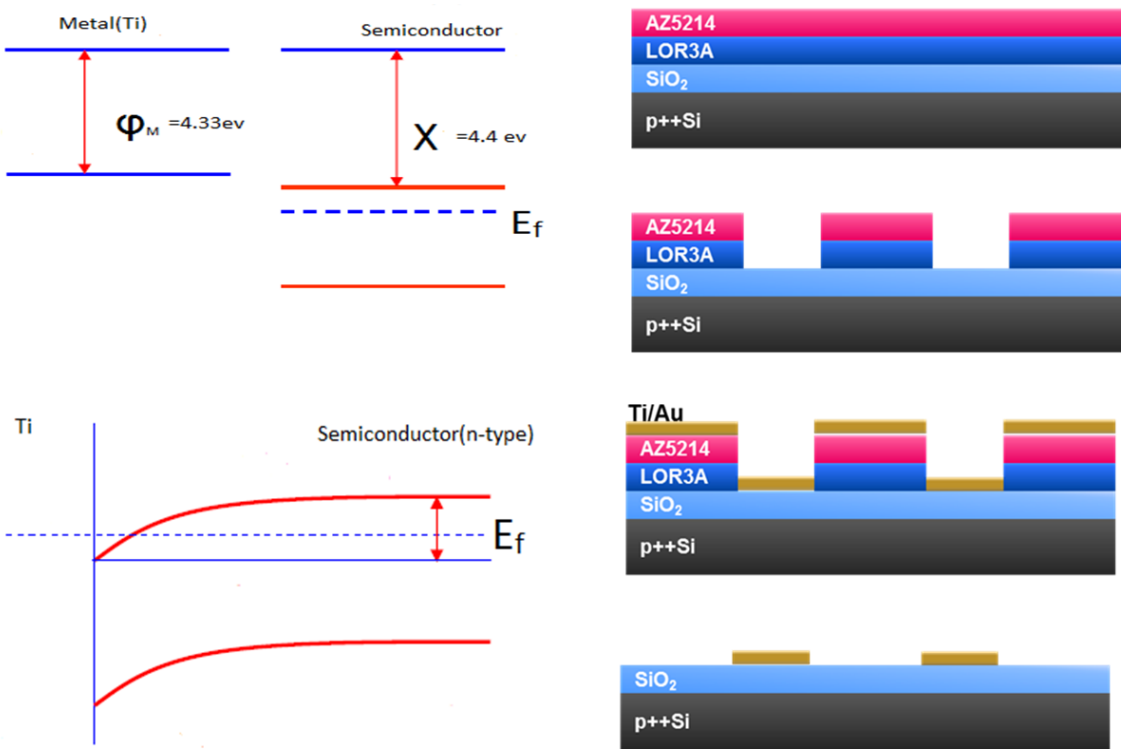

Figure 3.7 Band bending of semiconductor to achieve ohmic contact between CdS-Ti surface (left), and various steps involved in the nanowire device fabrications (right). The steps include deposition of photoresists, exposure, development of photoresist, metal deposition and lift off.

After liftoff, the devices are checked through the dark field imaging mode of the optical microscope in order to find the proper device to test. The proper device would be the one with nanowires spanning across at least two electrodes. Figure 3.8 shows the SEM image of a pattern of the device, and SEM images of the device with nanowires spanning across the electrodes. After confirming the devices, the dark current and photocurrent measurement of these devices are performed. These measurements are performed before and after the ligand binding in order to see the consequences of ligand binding on the nanowire surfaces.

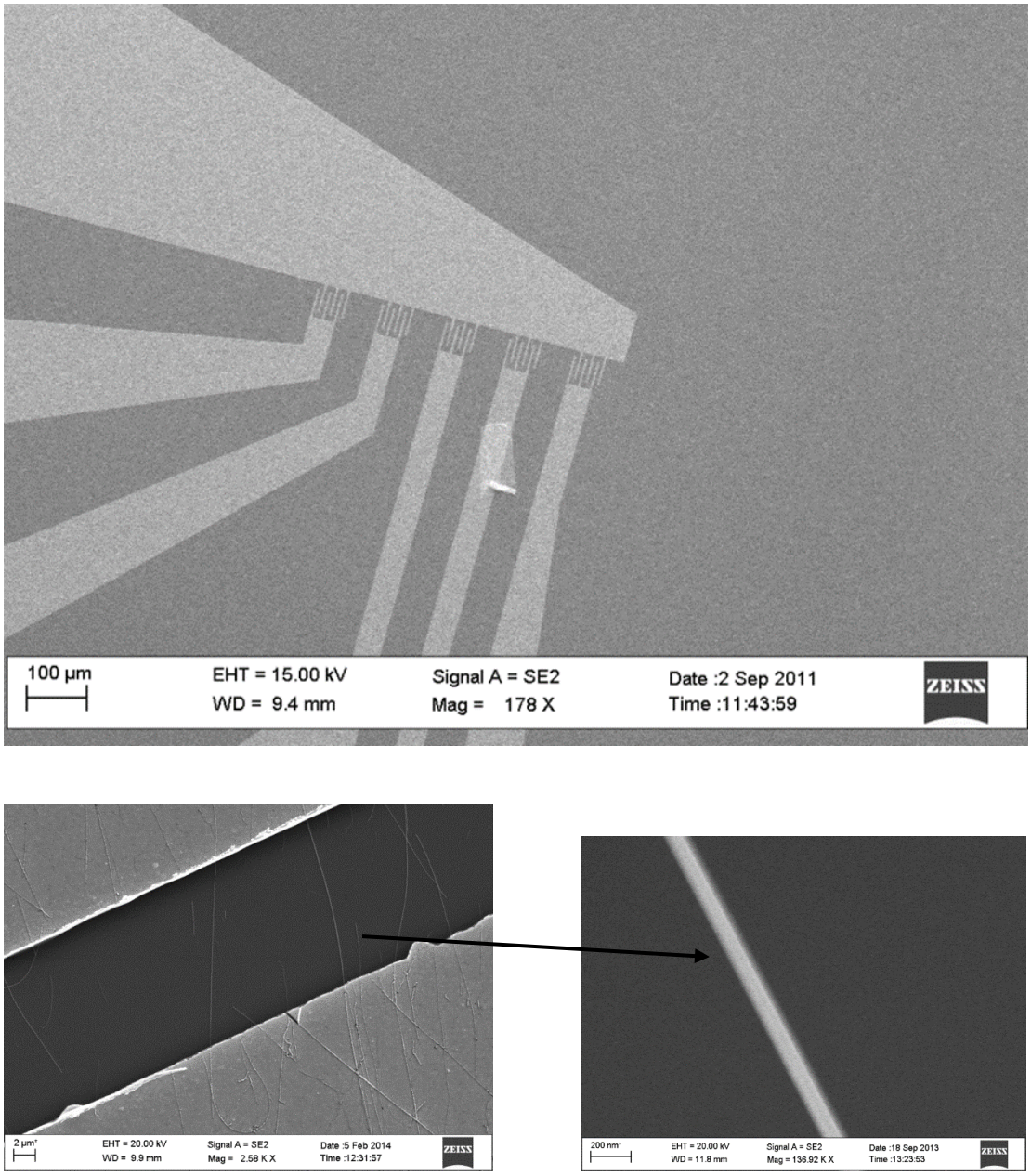

Figure 3.8 SEM image of the pattern of the device without nanowires (top) and nanowire device with the nanowire spanning across two electrodes (bottom). The diameter of nanowire is around 110 nm

3.3.2 Dark and photo current

After the identification of device, current voltage measurement is done with and without light. The current flowing through the length of nanowire is measured by applying the bias through electrodes. Not intentionally doped CdS nanowires have very low conductivity and higher noise level during measurement as shown in top of figure 3.9. Normally dark current is in nano- or sub- nano ampere range even at 10 V bias. This can be because of lower intrinsic carrier or non-ohmic nature of semiconductor-metal junction. In order to study the gate response on the current, we can look at the photocurrent, or we can do surface treatment to displace traps. However, when the nanowire is illuminated with laser light, the current increases significantly to micro ampere range (Figure 3.9, bottom). We achieved more than 2.5μA of current at 10 V. This photocurrent may be increased by binding ligands on the surface that can reduce surface states. We can look at the photocurrent with continuous excitation, or with the chopped excitation. Using a chopper to chop the light helps to isolate the photocurrent as well as provide information about carrier dynamics that can be used to calculate carrier lifetime.

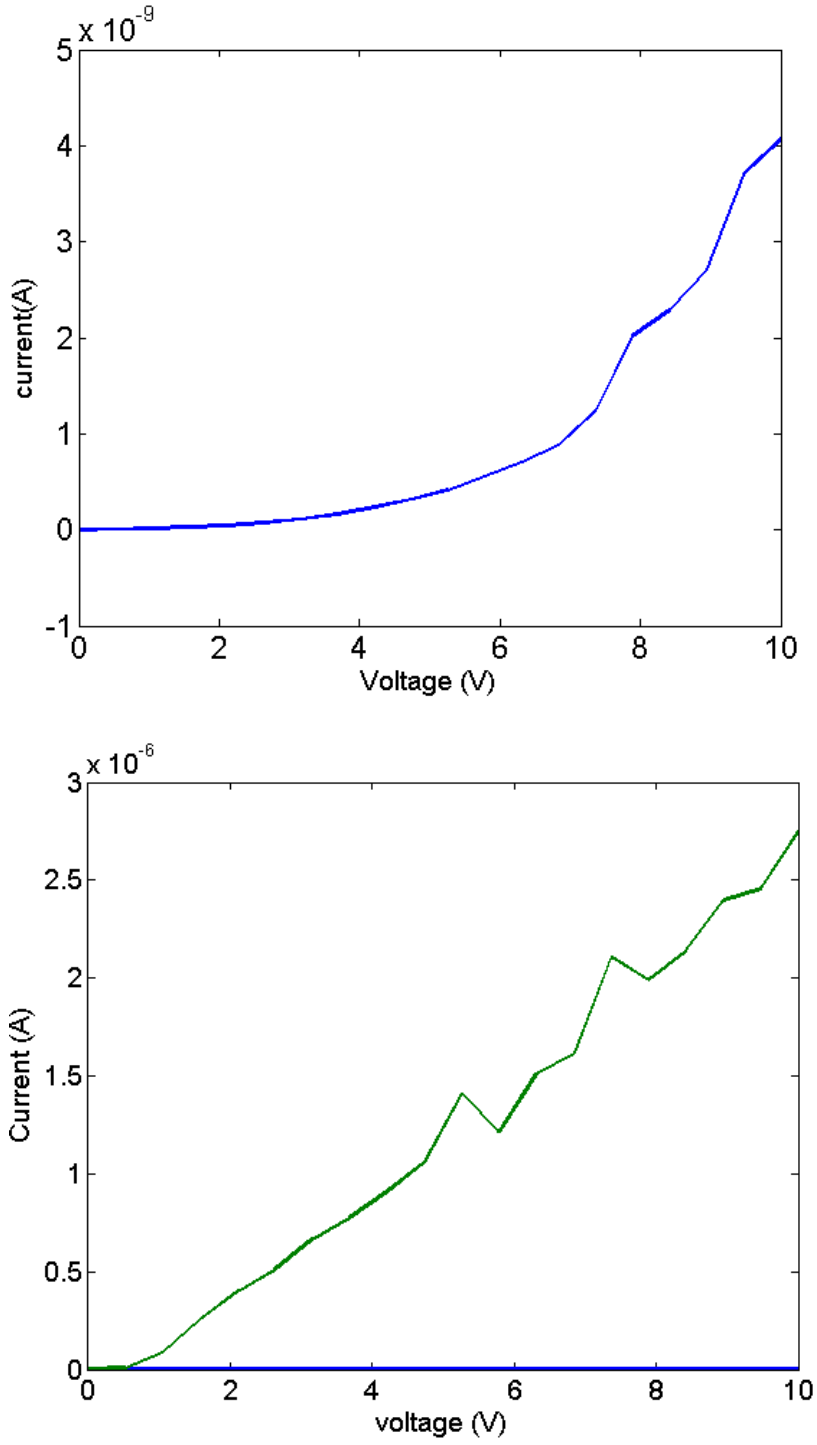

Figure 3.9 I-V curve of the CdS nanowire device without light (top),and I-V curve of the CdS device with (green), and without (blue)light. 440 nm laser was used with laser power 0.325 mW, and laser density 0.23 W/cm^2

3.3.3 Laser Chopping

By switching the laser light on and off, the photocurrent behavior and dark current can be studied. This measurement will allow us a direct comparison between photocurrent and dark current. This measurement is also important to study the effect of surface states in charge transfer and allow us to understand the mechanism of photocurrent decay. Figure 3.10 shows the total current with bias sweep. When the light is turned on, the total current rises significantly, and when light is turned off, it decreases significantly. However, when the light is turned off, we can see some kind of decay mechanism. We can use the decay time to calculate the carrier lifetime. From the graph 3.10, it can be seen that there are number of different decay mechanisms. The first rapid decays is hard to resolve, and there is another decay corresponding to around 50 milliseconds. By looking at the persistent photocurrent, we can be able to separate these decay mechanisms. This long decay of the charge carrier could be because of the surface states present on the nanowires, which is responsible to the persistent photocurrent, and possibly a photo gain.

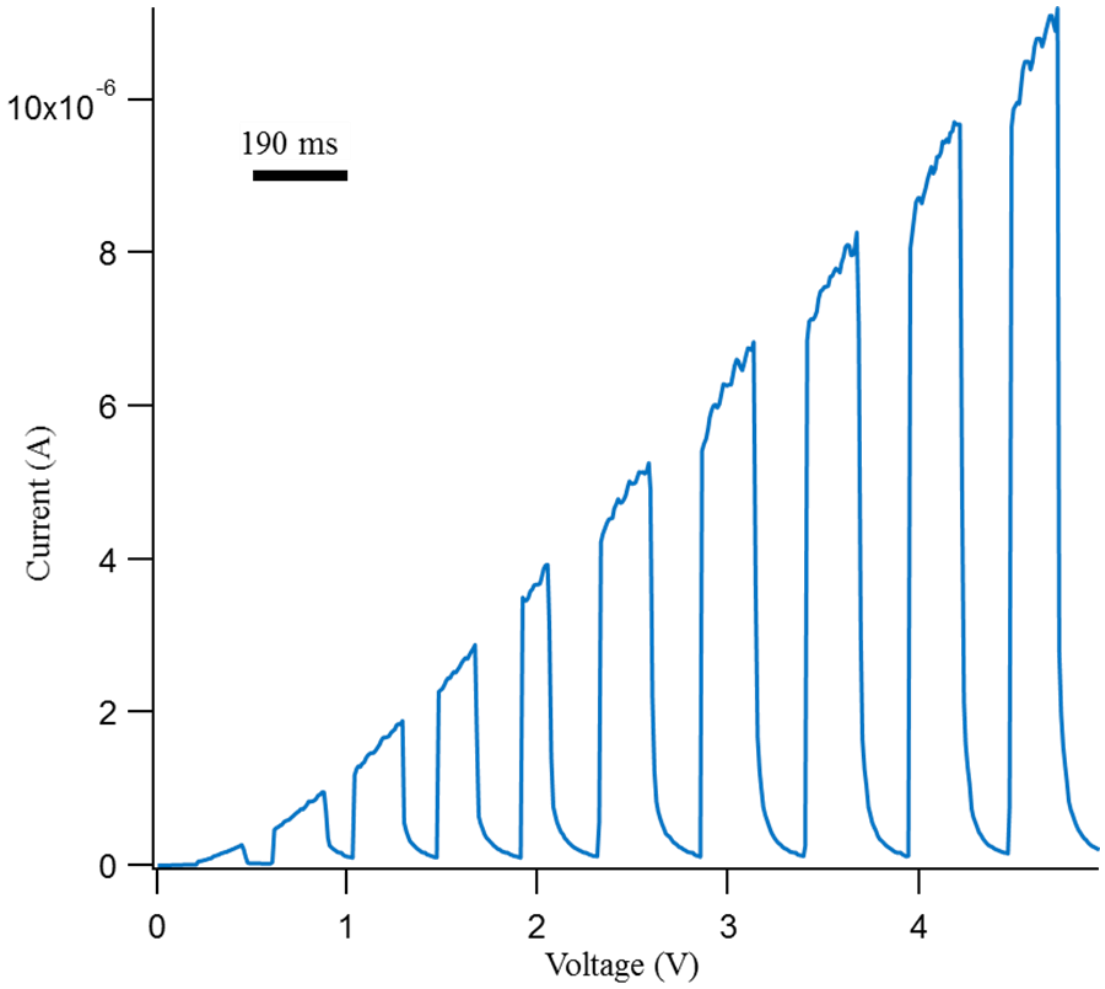

Figure 3.10 Total current of CdS nanowire device with respect to voltage. The light is turned on and off using the chopper. The illumination source is a laser diode with excitation wavelength of 440 nm.

3.3.4 Persistent photocurrent

Persistent photocurrent represents the presence of photocurrent even after the light source is terminated. This is very common phenomenon in semiconductor nanowires.[17] The presence of persistent photocurrent is because of the surface trap states which creates the surface potential by trapping the charges. It can be either by the surface states present in the semiconductor or by the crystal defect present in the material. CdS nanowires also exhibit persistent photocurrent for long time, up to few minutes. In case of bulk, exciton

lifetime of CdS crystal has been shown to be in nanosecond range.[18,19] However, our nanowires show longer persistent photocurrent. Figure 3.11 shows persistent photocurrent of CdS nanowires with respect to time at 10 V bias. A typical nanowire exhibit sub-nano ampere dark current. However, as seen in figure 3.11, even when light source is terminated, sub-micro ampere current is exhibited by nanowire for few minutes. It looks like there are three different characteristic lifetime of the excitons as evident by the chopped photocurrent measurement and persistent photocurrent. The first lifetime is in very small time frame, probably in nanoseconds. The other lifetime corresponds to around 100 seconds from which current drops from 0.8 microampere to 0.2 microampere. The third lifetime is very long, and it ranges from few minutes to few hours. The third lifetime decay is very slow as evident by the persistent photocurrent curve in figure 3.11. Persistent photocurrent measurements can be a good technique to detect the consequences of ligand binding on nanowire surface. In order to see if the ligands have been able to remove the surface state, this measurement can be performed before and after ligand binding on the nanowire surfaces.

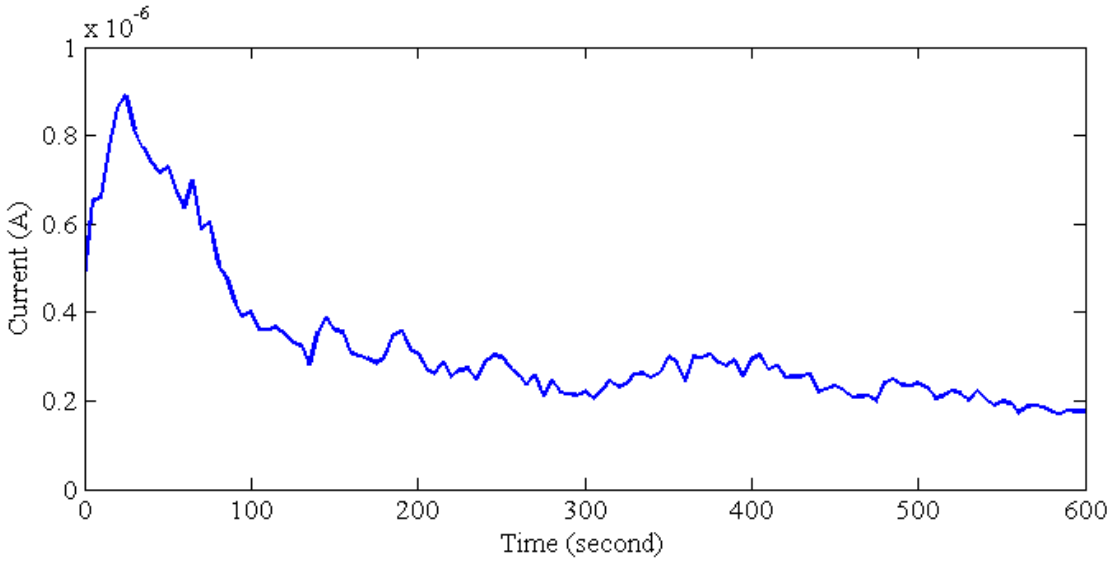

Figure 3.11 Persistent photocurrent of CdS nanowires at 10 V. The light source, diode laser with excitation wavelength at 440 nm was terminated at 0 second, and the measurement of current was performed for 600 seconds.

3.3.5 Dependence of current with Laser power

Dependence of the laser power on the total current at a particular bias is an important measurement to understand how effectively charge is being collected. The total current (dark current + photocurrent) depends on the charge carriers generated by the light as dark current is constant. The total current will increase with the increase in charge carriers. Therefore, the total current will increase with respect to the laser power showing linear curve. At higher illumination, the curve should be sub linear or flat because the number of available electron-hole at the surface is increasingly reduced reaching to the saturation of current.[17] However, if there is a recombination of charge carriers, which may be possible by the trap state, the curve will not be linear. Depending upon the bending of the curve, we can know if there is trap assisted recombination or persistent photocurrent produced by trapped charges. Top of figure 3.12 shows the curve of total

current with respect to voltage at different laser power using the chopper. The bottom curve shows the total current at 10 V with respect to different laser power. The curve is not completely linear, indicating charge recombination at low laser power.

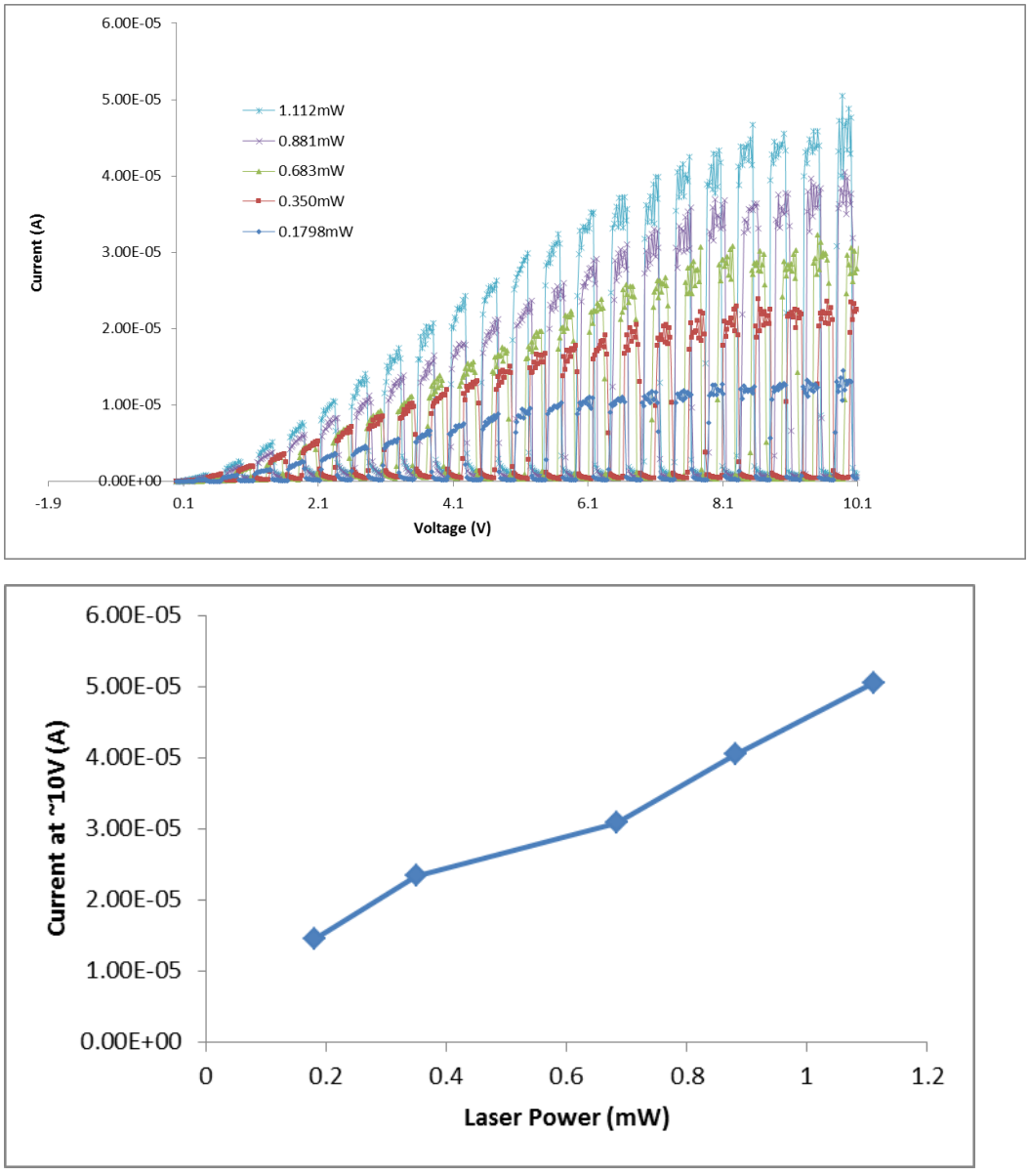

Figure 3.12 Dependence of total current with respect to laser power. The top curve shows the current with respect to voltage at different laser power with chopper on. The bottom curve shows the total current measured at 10 voltage with respect to the laser power. The excitation wavelength is 440 nm diode laser.

3.3.6 Treatment with CuCl

CuCl has been previously used on CdS nanowires to make CdS/Cu_2S heterojunction for photovoltaic applications.[20,21] When the nanowires are dipped in CuCl solution cation exchange takes place at the surface, that provides CdS core and Cu_2S shell. The same procedure was applied in our VLS grown CdS nanowires. After CdS nanowire device was fabricated, the dark current measurement was performed. The device was dipped in 0.5M CuCl solution for 10 seconds, and was rinsed with acetone, isopropanol, and DI water. The dark current measurement was performed again. Figure 3.13 shows the current of the device before and after treating with CuCl with respect to voltage. As grown CdS nanowire exhibits extremely low conductivity. However, when treated with CuCl, the current increases to micro ampere. A separate experiment done where only the contact region of nanowires are treated with the CuCl solution reveals the same increase in conductivity. The CdS has a band gap of 2.41 eV and Cu_2S has a band gap of 1.2 eV. When CdS and Cu_2S comes in contact, their fermi level has to match. While matching the fermi level, the electron from Cu_2S flows to CdS because the fermi level of Cu_2S is higher than poorly doped CdS. This increases the charge carrier yielding larger current. The band diagram of CdS and Cu_2S, and the representative structure of CdS/Cu_2S is shown in figure 3.14 when they come in contact. Figure 3.15 shows the gate response of the representative nanowire field effect transistor device. It can be seen that with an increase in the gate voltage, the current also increases. This represents the n type conductivity of the nanowire device.

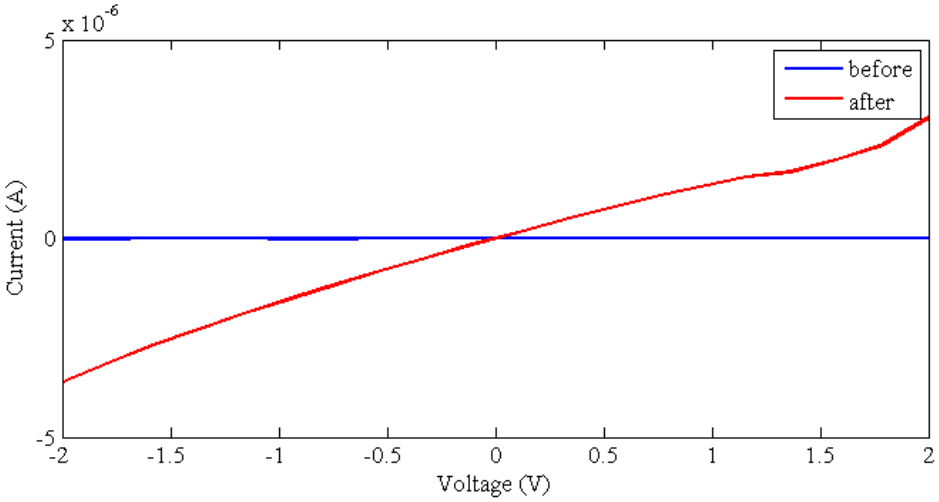

Figure 3.13 Dark current of CdS nanowire before and after the treatment with CuCl with respect to voltage. Blue line represents current before surface treatment, and red line represents current after the surface treatment.

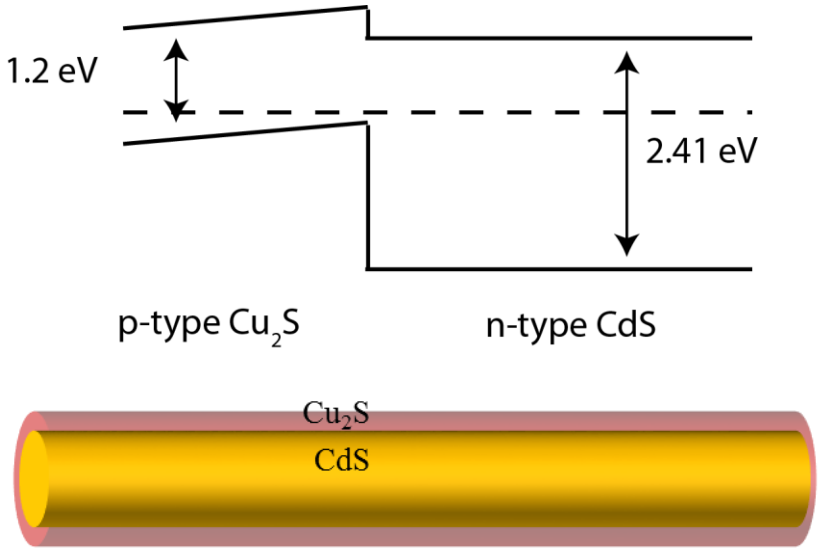

Figure 3.14 Energy band diagram of p-Cu_2S and n-CdS when they come in contact, and schematic of Cds/Cu_2S heterostructure

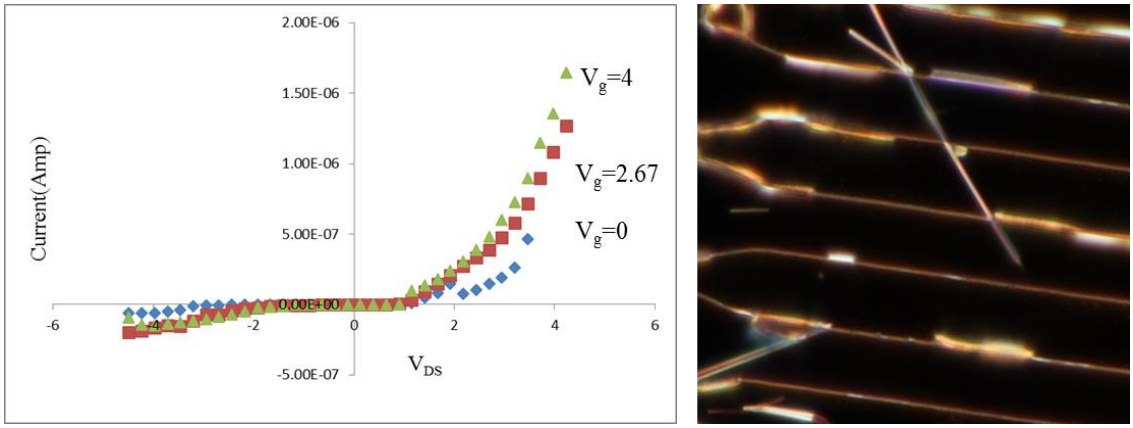

Figure 3.15 Gate response of a representative nanowire field-effect transistor. The nanowire is treated with CuCl, and I-V measurement is done at 0, 2.67, and 4 gate voltage.

3.3.7 Surface treatment with cadmium acetate

In the case of SLS grown CdSe nanowires, it has been shown that treating CdSe nanowires with cadmium acetate makes Cd rich surfaces which passivates the surface and removes surface states created by unsaturated atoms at surface, that enhances the electron current of the device.[22] We chose VLS grown CdS nanowires to see the consequences of cadmium acetate treatment in the photocurrent of the device.

The photocurrent measurement of as grown nanowire was performed using a 440 nm diode laser. The nanowire device was dipped in 50 mM cadmium acetate solution in dry methanol for 10 minutes inside the glove box. The nanowire device was then rinsed with fresh dry methanol and dried with nitrogen gas. A photocurrent measurement was performed to see the effect of cadmium doping. Figure 3.16 shows the total current of the nanowire device before (blue) and after treating with cadmium acetate. It can be clearly seen that the current increases significantly after treating the surface with cadmium

acetate. It suggests the removal of surface state created because of unsaturated atoms at the surface.

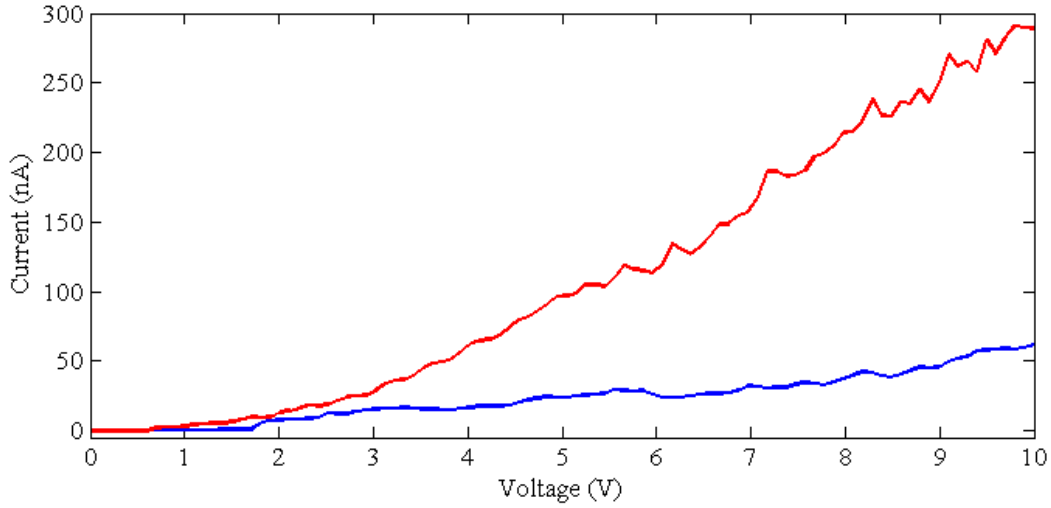

Figure 3.16 I-V curve of CdS nanowires before (blue) and after (red) treating with cadmium acetate solution. The excitation source is a 440 nm diode laser.

3.4 CONCLUSION

Controlling the interfaces of nanowires is an integral part of nanowire electronics. These interfaces can be controlled by binding ligands on the nanowire surfaces. These ligands control various electronic and optical properties of nanowires. Photoluminescence measurement and transport measurements can be performed to study the consequences of ligand binding. Photoluminescence measurement indicates the recombination pathways of the charge carrier, and transport measurement can provide the insight of how efficiently these charges are being extracted.

We have been able to show an increase in photoluminescence and conductivity by binding various ligands on the nanowire surface. However, these experiments may not be repeatable depending on the surface termination of nanowire. Therefore, it is very important to understand how the surface is terminated. Various HR-TEM imaging can be

done to better understand the surface of nanowires after growth. Similarly, Oxygen free atmosphere needs to be used to perform the surface chemistry and measurements. In the presence of oxygen, surface may be terminated with oxide which might hinder access to the ligands resulting in poor conductivity.

References

(1) Gu, Y.; Lauhon, L. J. *Appl. Phys. Lett.* **2006**, *89* (14), 143102.

(2) Gomes, R.; Hassinen, A.; Szczygiel, A.; Zhao, Q.; Vantomme, A.; Martins, J. C.; Hens, Z. *J. Phys. Chem. Lett.* **2011**, *2* (3), 145–152.

(3) Owen, J. S.; Park, J.; Trudeau, P.-E.; Alivisatos, A. P. *J. Am. Chem. Soc.* **2008**, *130* (37), 12279–12281.

(4) Rosenthal, S. J.; McBride, J.; Pennycook, S. J.; Feldman, L. C. *Surf. Sci. Rep.* **2007**, *62* (4), 111–157.

(5) Peng, Z. A.; Peng, X. *J. Am. Chem. Soc.* **2001**, *123* (1), 183–184.

(6) Schreuder, M. A.; McBride, J. R.; Dukes, A. D.; Sammons, J. A.; Rosenthal, S. J. *J. Phys. Chem. C* **2009**, *113* (19), 8169–8176.

(7) Liu, W.; Choi, H. S.; Zimmer, J. P.; Tanaka, E.; Frangioni, J. V.; Bawendi, M. *J. Am. Chem. Soc.* **2007**, *129* (47), 14530–14531.

(8) Zhang, Y.; Clapp, A. *Sensors* **2011**, *11* (12), 11036–11055.

(9) Park, C.; Yoon, T. H. *Colloids Surf. B Biointerfaces* **2010**, *75* (2), 472–477.

(10) Shen, Y.; Gee, M. Y.; Tan, R.; Pellechia, P. J.; Greytak, A. B. *Chem. Mater.* **2013**, *25* (14), 2838–2848.

(11) Yun, H. J.; Paik, T.; Edley, M. E.; Baxter, J. B.; Murray, C. B. *ACS Appl. Mater. Interfaces* **2014**, *6* (5), 3721–3728.

(12) Hanrath, T.; Korgel, B. A. *J. Am. Chem. Soc.* **2004**, *126* (47), 15466–15472.

(13) Adhikari, H.; McIntyre, P. C.; Sun, S.; Pianetta, P.; Chidsey, C. E. D. *Appl. Phys. Lett.* **2005**, *87* (26), 263109.

(14) Knowles, K. E.; Tice, D. B.; McArthur, E. A.; Solomon, G. C.; Weiss, E. A. *J. Am. Chem. Soc.* **2010**, *132* (3), 1041–1050.

(15) Murphy, C. J.; Lisensky, G. C.; Leung, L. K.; Kowach, G. R.; Ellis, A. B. *J. Am. Chem. Soc.* **1990**, *112* (23), 8344–8348.

(16) Gu, Y.; Romankiewicz, J. P.; David, J. K.; Lensch, J. L.; Lauhon, L. J.; Kwak, E.-S.; Odom, T. W. *J. Vac. Sci. Technol. B* **2006**, *24* (4), 2172–2177.

(17) Soci, C.; Zhang, A.; Xiang, B.; Dayeh, S. A.; Aplin, D. P. R.; Park, J.; Bao, X. Y.; Lo, Y. H.; Wang, D. *Nano Lett.* **2007**, *7* (4), 1003–1009.

(18) Henry, C. H.; Nassau, K. *Phys. Rev. B* **1970**, *1* (4), 1628–1634.

(19) Korotchenkov, O. A.; Goto, T. *Appl. Phys. Lett.* **1998**, *72* (14), 1733–1735.

(20) Tang, J.; Huo, Z.; Brittman, S.; Gao, H.; Yang, P. *Nat. Nanotechnol.* **2011**, *6* (9), 568–572.

(21) Pan, C.; Niu, S.; Ding, Y.; Dong, L.; Yu, R.; Liu, Y.; Zhu, G.; Wang, Z. L. *Nano Lett.* **2012**, *12* (6), 3302–3307.

(22) Kim, D. K.; Fafarman, A. T.; Diroll, B. T.; Chan, S. H.; Gordon, T. R.; Murray, C. B.; Kagan, C. R. *ACS Nano* **2013**, *7* (10), 8760–8770.

CHAPTER 4

TRANSPORT MEASUREMENT OF IODINE DOPED POLYDIACETYLENE (PDA) MICROFIBERS

4.1 INTRODUCTION

Carbon nanotubes are widely studied because of their unique electrical[1], mechanical[2] and thermal[3] properties which make them a good candidate in various electronic devices. Polydiacetylene (PDA) fibers are a class of carbon-based nanotubes with properties tunable by modifying the monomer, or by doping with the guest molecules. These tunable properties make them applicable in various organic electronic devices including organic photovoltaics[4], organic light emitting diode[5], and sensors[6]. These fibers are highly porous materials, which make them an interesting candidates for studying the effect of guest intercalation.

PDAs are synthesized by thermal polymerization or UV-irradiation of a diacetylene monomer assembled in to columns through supramolecular interactions[7]. This polymerization process is a single crystal to single crystal polymerization[7]. These bundles of PDA nanotubes connected by amide bonds form the PDA fibers. These fibers consist of chain of alternating enes-ynes which make them capable of electrical conductivity, subject to various environmental conditions like temperature, pH, and guest interactions.

Figure 4.1 shows four individual nanotubes connected by amide bonds and an optical image of PDA fibers. The crystal structure was obtained through X-Ray diffraction, and the data were collected on a Bruker SMART APEX diffractometer with Mo kα radiation.

PDA fibers are quasi one dimensional semiconductor materials with wide a band gap of 2.0 eV[8] and a high density of states at the band edge[9]. It has been shown that bulk PDA film shows fast photoconduction properties, and a nonlinear response[8] . By doping those PDAs with small molecules, these properties can be altered and higher conductivity can be achieved[8].

This work focuses on the effect of guest intercalation in particular introduction of a guest iodine that can alter the electronic properties of PDA fibers. PDA fibers are doped with iodine molecules, and the change in electronic and optical properties are studied by organic field effect transistor measurements, and fluorescence spectroscopy. The electronic studies shows the change in conductivity after doping PDAs with iodine, and by fluorescence spectroscopy shows wide emission after doping.

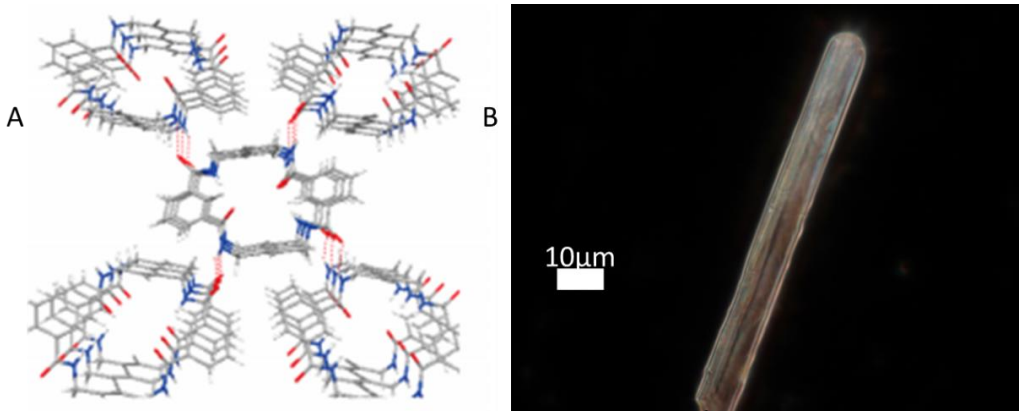

Figure 4.1 structure and Morphology of PDA fibers. A) Structure of four PDA nanotubes connected by amide bond as obtained from XRD B) Dark field scattered image of PDA fibers.

4.2 DEVICE FABRICATION

To study the axial transport properties of PDA fibers, organic field effect transistor structures were fabricated. Because of large size of macrocycle fibers, bottom contact[10] was used by designing metal electrode pattern on a Si substrate with 400 nm oxides surface. Photolithography was performed in the substrate using LOR3A and AZ5214 to obtain a designed pattern, and Ti/Au (30nm/70nm) metal was deposited as an electrode. The details of the device fabrication are explained in chapter 3. Figure 4.2A shows the steps involved during photolithography and metal deposition, Figure 4.2B shows the representative electrode pattern, and figure 4.2C shows the schematic of the device.

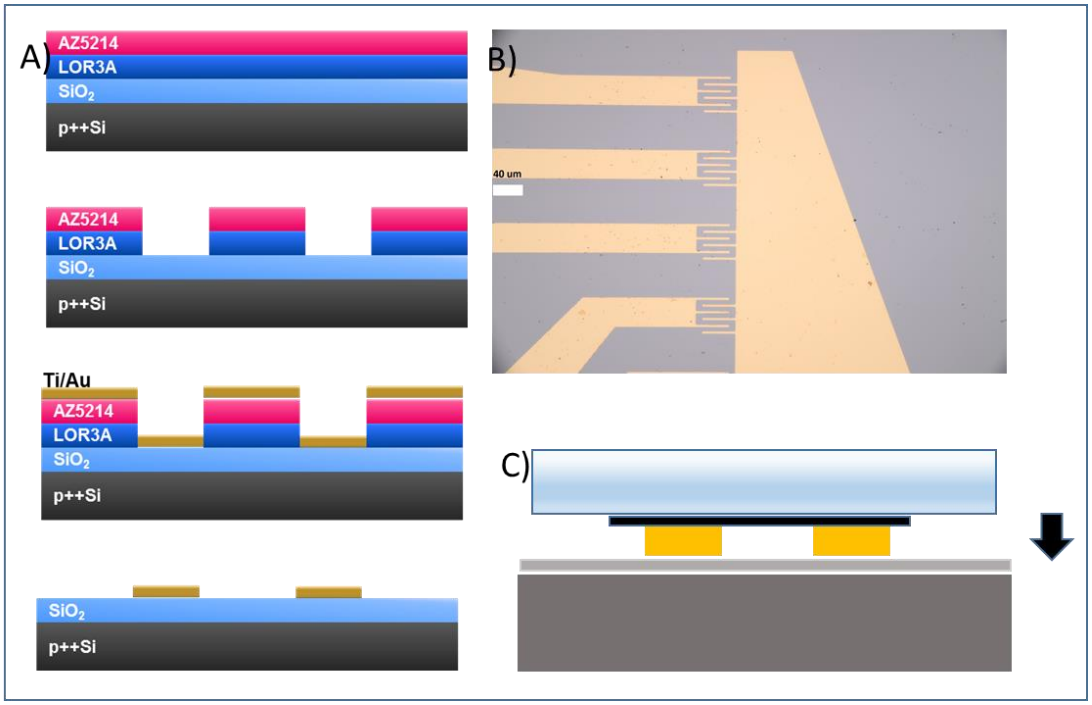

Figure 4.2: Device fabrication and design scheme to study axial transport of PDA fibers. Figure A shows the steps involved in fabrication of device. B shows the test pattern of the device. C shows schematic of the device

4.3 MEASUREMENTS

In order to study the charge transport in PDA fibers, an individual microfiber was selected and oriented such a way that it span two electrodes. The fiber was pressed by Polydimethyl siloxane (PDMS) stamp as shown in Figure 4.3. The transport properties were studied using probe station and a Keithley 2636A source meter.

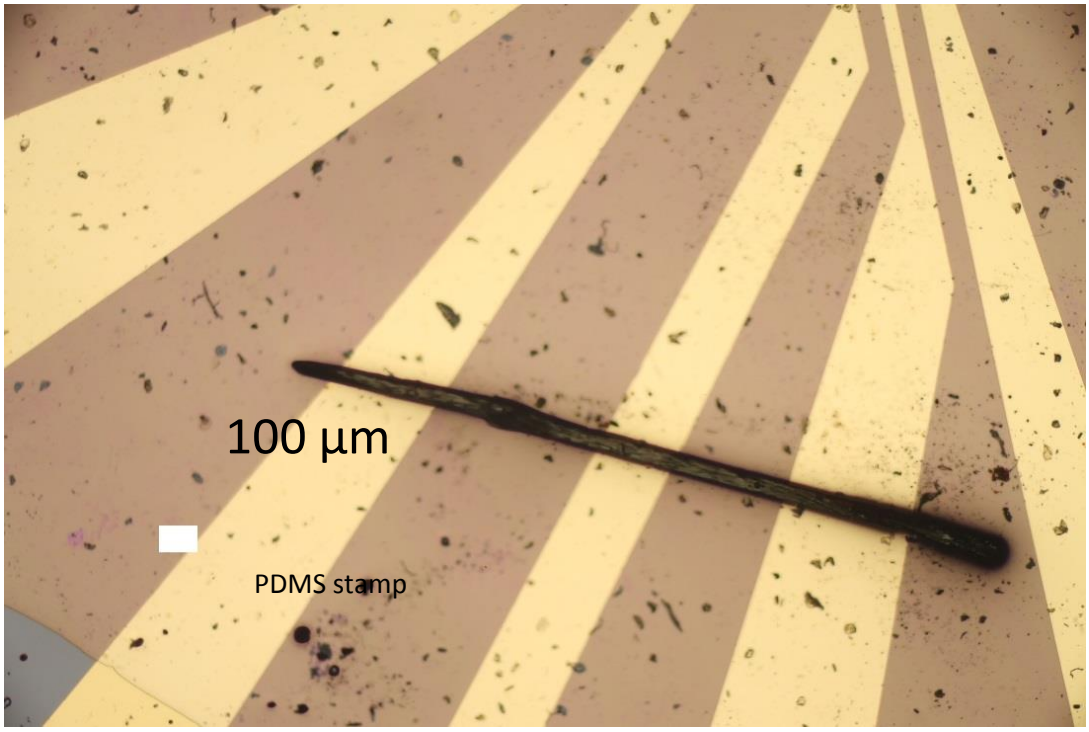

Figure 4.3: Microscopy image of PDA fibers pressed with PDMS stamp to span through three electrodes.

4.4 IODINE DOPING

Iodine was doped in PDA fibers by passing iodine vapor at room temperature in the iodine loading chamber containing fibers. The schematic of the iodine doping system is shown in Figure 4.4. A known amount of nitrogen was passed through the iodine chamber to obtain iodine vapor. The mixture of iodine vapor and nitrogen gas was supplied to iodine loading chamber containing PDA fibers and an outlet. No iodine crystal was observed in the iodine loading chamber confirming that the partial pressure of iodine in the sample chamber does not exceed the equilibrium vapor pressure. Iodine doping was confirmed by X-ray photoelectron spectroscopy (XPS). XPS of iodine doped fibers reveal two extra peaks that corresponds to iodine.

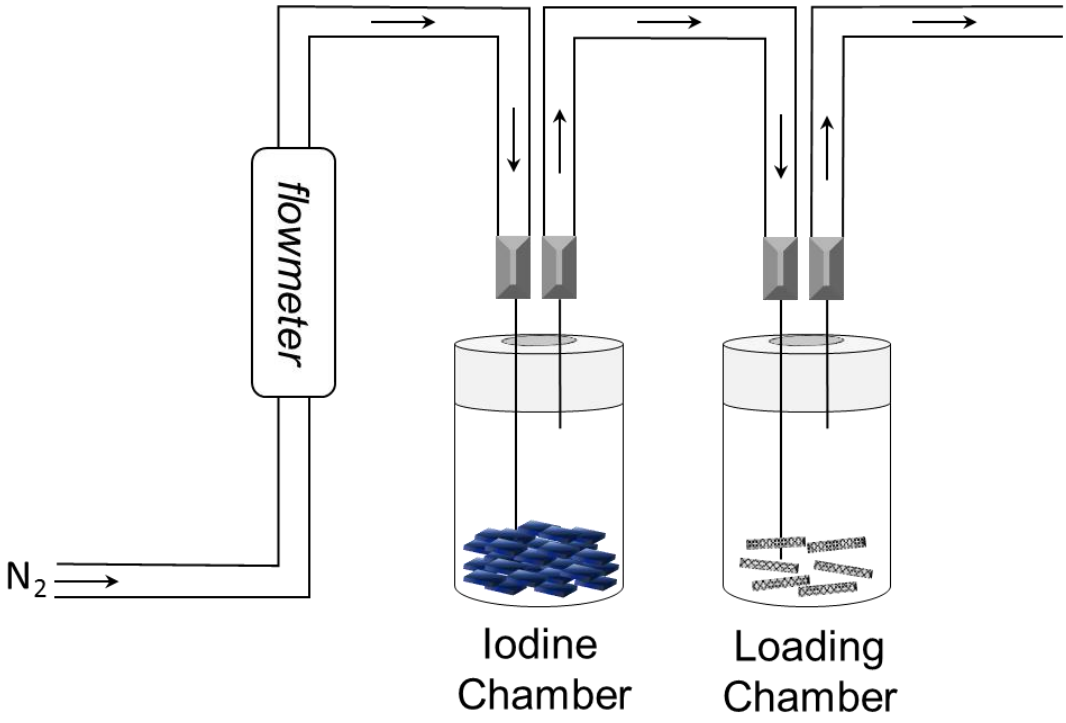

Figure 4.4: schematic of iodine doping system showing iodine chamber and iodine loading chamber

4.5 RESULTS

Current-voltage measurement of undoped PDA fibers showed these fibers have negligible conductivity. After overnight (12 hrs.) iodine vapor loading on these fibers, they show higher conductance. Upon doping with iodine, iodine gets reduced, generating unlocalized holes which contributes to the conductivity. Figure 4.5 shows the conductance of representative doped and undoped fibers. We can see the conductance of undoped fibers is much less compared to doped ones. It is clearly evident that after doping the fibers with iodine, the fibers become more conductive. Using a significance level of 0.05, for a two tailed test the *p* value was calculated to be 0.011 which shows significant difference in the conductivity of doped and undoped fibers. Figure 4.6 shows

the representative I-V curve of doped and undoped micro fibers. The blue curve is the *I-V* curve of doped fibers, and green curve represents *I-V* curve of undoped fibers. Among the examples tested, the highest conductivity was found in a PDA fiber with length (between contacts) of 420 μm, and a diameter of 55 μm, the conductivity is calculated to be 6.69 μS/cm. No dependence of current on gate voltage was detected; gate was held at ground during the application of bias voltage. The fibers are weakly fluorescent when excited at 365 nm. The fluorescence spectrum taken from the undoped and doped fibers also show clear slight blue shift in the peak position, and widening of the peaks upon introduction of iodine as seen in figure 4.7.

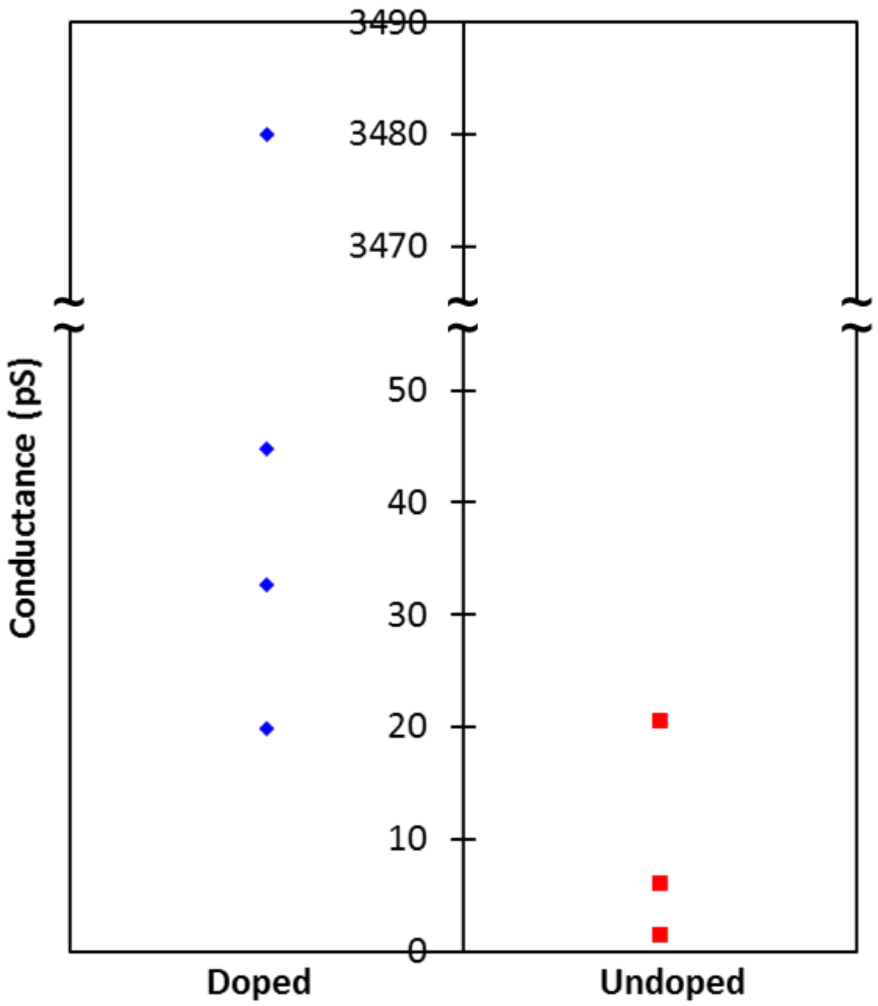

Figure 4.5: comparison of conductance of doped and undoped Microfibers at 20 V.

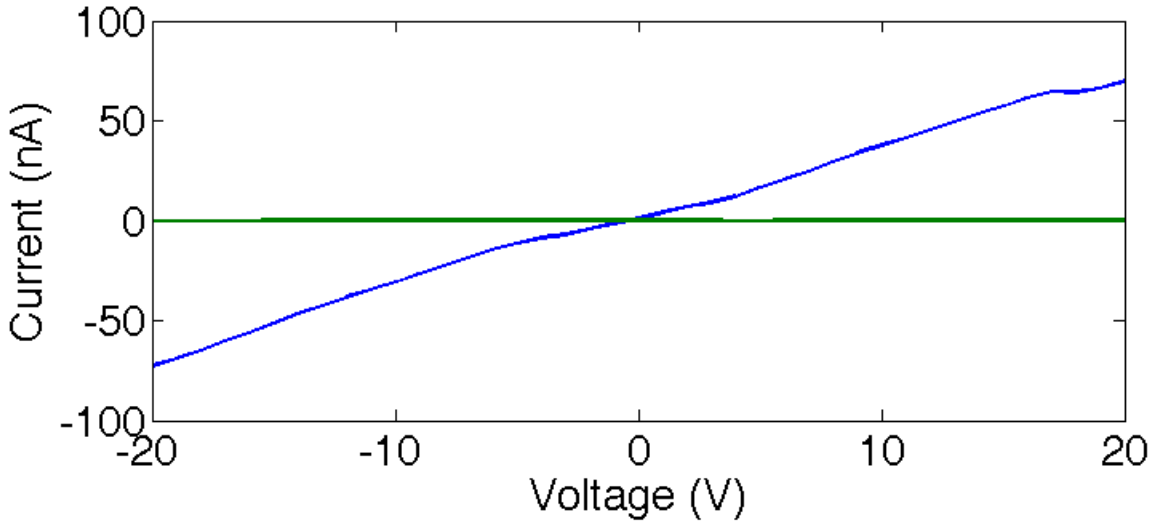

Figure 4.6: I-V curve of doped (blue), and undoped (green) PDA fibers

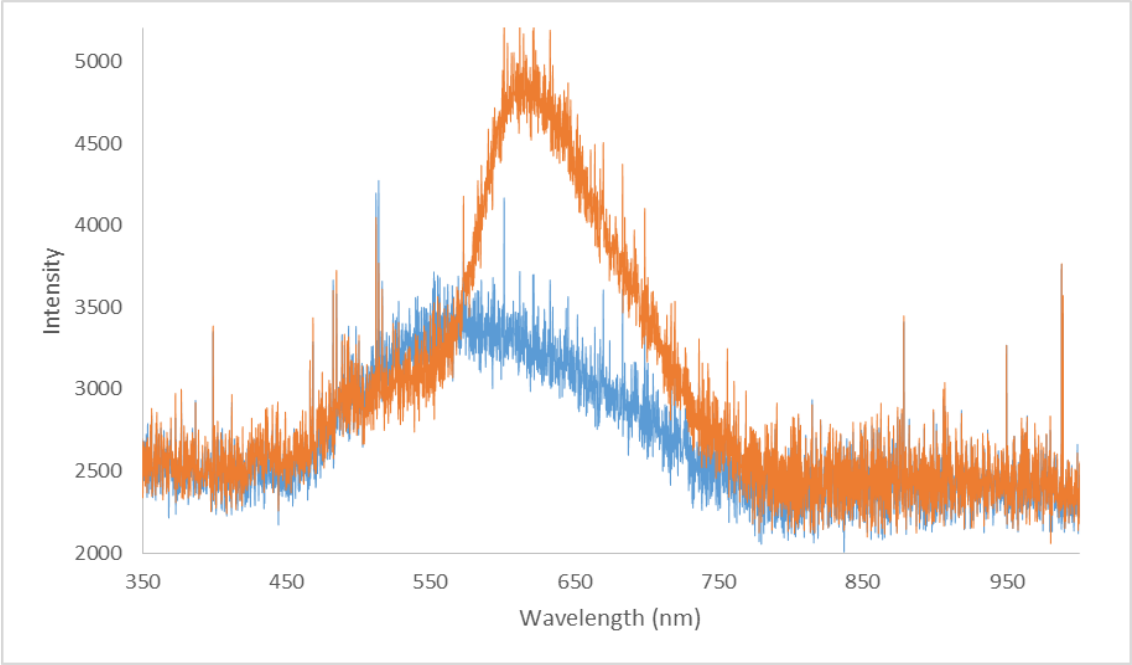

Figure 4.7: Fluorescence spectrum of undoped (orange), and doped (blue) PDA fibers under 365 nm excitation

4.6 CONCLUSIONS

The Transport properties of doped and undoped PDA fibers were studied. It was shown that doping the PDA fibers changes the electronic and optical properties of PDA fibers. Doping the fibers increases the conductivity of the fibers. This change in the electronic behavior can open the possibility of using those fibers as a future of organic electronic devices**.**

References:

(1) Hu, P.; Zhang, J.; Li, L.; Wang, Z.; O'Neill, W.; Estrela, P. *Sensors* **2010**, *10* (5), 5133–5159.

(2) Diao, P.; Liu, Z. *Adv. Mater.* **2010**, *22* (13), 1430–1449.

(3) Cahill, D. G.; Ford, W. K.; Goodson, K. E.; Mahan, G. D.; Majumdar, A.; Maris, H. J.; Merlin, R.; Phillpot, S. R. *J. Appl. Phys.* **2003**, *93* (2), 793–818.

(4) Antoniadis, H.; Hsieh, B. R.; Abkowitz, M. A.; Jenekhe, S. A.; Stolka, M. *Synth. Met.* **1994**, *62* (3), 265–271.

(5) Gather, M. C.; Köhnen, A.; Meerholz, K. *Adv. Mater.* **2011**, *23* (2), 233–248.

(6) Swager, T. M. *Acc. Chem. Res.* **1998**, *31* (5), 201–207.

(7) Xu, W. L.; Smith, M. D.; Krause, J. A.; Greytak, A. B.; Ma, S.; Read, C. M.; Shimizu, L. S. *Cryst. Growth Des.* **2014**, *14* (3), 993–1002.

(8) Day, D. R.; Lando, J. B. *J. Appl. Polym. Sci.* **1981**, *26* (5), 1605–1612.

(9) Mahato, R. N.; Lülf, H.; Siekman, M. H.; Kersten, S. P.; Bobbert, P. A.; Jong, M. P. de; Cola, L. D.; van der Wiel, W. G. *Science* **2013**, *341* (6143), 257–260.

(10) Sundar, V. C.; Zaumseil, J.; Podzorov, V.; Menard, E.; Willett, R. L.; Someya, T.; Gershenson, M. E.; Rogers, J. A. *Science* **2004**, *303* (5664), 1644–1646.